

Collective enhancement and suppression in Bose-Einstein condensates

Wolfgang Ketterle and Shin Inouye

*Department of Physics and Research Laboratory of Electronics,
Massachusetts Institute of Technology, Cambridge, MA 02139, USA*

(May 1, 2019)

The coherent and collective nature of a Bose-Einstein condensate can enhance or suppress physical processes. Bosonic stimulation enhances scattering in already occupied states which leads to matter wave amplification, and the suppression of dissipation leads to superfluidity. In this summer school notes we present several experiments where enhancement and suppression have been observed and discuss the common roots of and differences between these phenomena.

Contents

I	Scattering of light and massive particles	2
II	Determination of the static structure factor by Bragg spectroscopy	4
III	Atomic collisions in a Bose-Einstein condensate	6
IV	Suppression of impurity collisions	9
V	Suppression of dissipation for a moving macroscopic object	12
VI	Four-wave mixing of light and atoms	15
VII	Superradiance and matter wave amplification	17
VIII	Amplification of light in a dressed condensate	19
	A Cross-section for optical gain and slow light	20
	B Relation between optical gain and atomic gain	21
	C Optical Bloch equations	23
	D Optical probe of matter wave gain	26
	E Single-atom and collective behavior	26
IX	Enhancement of spontaneous emission in a Bose-Einstein condensate	30
X	Does matter wave amplification work for fermions?	32
XI	Discussion	36

arXiv:cond-mat/0101424v1 [cond-mat.soft] 29 Jan 2001

When a gas of bosonic atoms is cooled below the transition temperature of Bose-Einstein condensation, it profoundly changes its properties. The appearance of a macroscopically occupied quantum state leads to a variety of new phenomena which set quantum fluids apart from all other substances. Fritz London even called them the fourth state of matter [1].

Many of the key concepts in quantum fluids were derived from studying the weakly interacting Bose gas, for which rigorous theoretical treatments were possible [2,3]. In 1995, with the discovery of BEC in a dilute gas of alkali atoms [4–6], it became possible to study such a system experimentally. Since then, the interplay between theory and experiment has been remarkable [7].

This paper is the fourth major review paper of our group which describes the new techniques and the physics of Bose-Einstein condensation [8–10]. These review papers together give a comprehensive overview of the topics to which our group has contributed. Each contribution is self-contained, but we avoided major overlap with previous review papers. The topic of these Cargèse summer school notes is enhancement and suppression of physical processes in a Bose-Einstein condensate.

Many phenomena in Bose condensates involve such enhancement or suppression. Our recent experiments include the enhancement and suppression of elastic collisions of impurity atoms [11], the suppression of dissipation due to superfluidity [12,13], and the enhancement [14] and suppression [15] of light scattering. The common discussion of these phenomena leads to a better understanding of the underlying principles. We draw analogies between light scattering and particle scattering, between microscopic and macroscopic superfluidity. We show that a condensate responds very differently to two different ways of momentum transfer, light scattering and spontaneous emission [16]. We discuss light scattering in both the linear and nonlinear regime where bosonically enhanced Rayleigh scattering led to the amplification of either atoms [17] or light [18] and work out the relationship between these two processes. Finally, the section on matter wave amplification of fermions discusses the relevance of symmetry and long coherence time and its relation to quantum statistics.

I. SCATTERING OF LIGHT AND MASSIVE PARTICLES

Before we discuss light scattering and collisions in a BEC, we want to derive some simple general expressions based on Fermi's golden rule. This will help to see the similarities and differences between the various processes. When a condensate scatters a photon or material particle, the scattering is described by the Hamiltonian

$$\mathcal{H}' = C \sum_{k,l,m,n} \hat{c}_l^\dagger \hat{a}_n^\dagger \hat{c}_k \hat{a}_m \delta_{l+n-k-m}. \quad (1)$$

Here \hat{c}_k (\hat{c}_k^\dagger) is the destruction (creation) operator for the scattered particles (which can be photons or massive particles), and \hat{a}_k (\hat{a}_k^\dagger) is the destruction (creation) operator for atomic plane waves of wavevector \mathbf{k} (free particle states). The strength of the coupling is parametrized by the coefficient C (which in general may depend on the momentum transfer), and the δ function guarantees momentum conservation (with an uncertainty of \hbar/D , where D is the dimension of the condensate).

We consider the scattering process where a system with N_0 atoms in the condensate ground state and N_q quasi-particles with wavevector \mathbf{q} scatters particles with incident wavevector \mathbf{k} into a state with wavevector $\mathbf{k} - \mathbf{q}$. The initial and final states are¹

$$\begin{aligned} |i\rangle &= |n_{\mathbf{k}}, n_{\mathbf{k}-\mathbf{q}}; N_0, N_q\rangle \\ |f\rangle &= |n_{\mathbf{k}} - 1, n_{\mathbf{k}-\mathbf{q}} + 1; N_0 - 1, N_q + 1\rangle \end{aligned} \quad (2)$$

respectively, where $n_{\mathbf{k}}$ denotes the population of scattering particles with wavevector \mathbf{k} . It should be emphasized that, due to the interatomic interactions, the quasi-particles with occupation N_q are not the plane waves created by the operator \hat{a}_q^\dagger , but the quanta of collective excitations with wavevector \mathbf{q} .

The square of the matrix element M_1 between the initial and final state is

¹This choice of final states implies that we neglect scattering between quasi-particles and consider only processes involving the macroscopically occupied zero-momentum state of the condensate. Formally, we replace the Hamiltonian (Eq. 1) by $C \sum_{k,q} (\hat{c}_{k-q}^\dagger \hat{a}_q^\dagger \hat{c}_k \hat{a}_0 + \hat{c}_{k-q}^\dagger \hat{a}_0^\dagger \hat{c}_k \hat{a}_{-q})$.

$$\begin{aligned}
|M_1|^2 &= |\langle f | \mathcal{H}' | i \rangle|^2 \\
&= |C|^2 |\langle N_0 = N - 1, N_q = 1 | \hat{\rho}^\dagger(\mathbf{q}) | N_0 = N, N_q = 0 \rangle|^2 (N_q + 1)(n_{k-q} + 1)n_k
\end{aligned} \tag{3}$$

where $\hat{\rho}^\dagger(\mathbf{q}) = \sum_m \hat{a}_{m+q}^\dagger \hat{a}_m$ is the Fourier transform of the atomic density operator at wavevector \mathbf{q} . The static structure factor of the condensate is

$$S(q) = \langle g | \hat{\rho}(\mathbf{q}) \hat{\rho}^\dagger(\mathbf{q}) | g \rangle / N \tag{4}$$

where $|g\rangle = |N_0 = N, N_q = 0\rangle$ is the BEC ground state and N is the total number of atoms. We then obtain for the scattering matrix element M_1

$$|M_1|^2 = |C|^2 S(q) (N_q + 1)(n_{k-q} + 1) N_0 n_k. \tag{5}$$

The scattering rate W_1 for the process $|n_k, n_{k-q}; N_0, N_q\rangle \rightarrow |n_k - 1, n_{k-q} + 1; N_0 - 1, N_q + 1\rangle$ follows from Fermi's golden rule as

$$W_1 = \frac{2\pi}{\hbar} |M_1|^2 \delta(E_k - E_{k-q} - \hbar\omega_q^B) \tag{6}$$

where E_k is the energy of the incident particle with wavevector \mathbf{k} , and $\hbar\omega_q^B$ is the energy of quasi-particles with wavevector \mathbf{q} (which we will later obtain from Bogoliubov theory). To obtain the net growth rate of N_q , one has to include the reverse process $|n_k, n_{k-q}; N_0, N_q\rangle \rightarrow |n_k + 1, n_{k-q} - 1; N_0 + 1, N_q - 1\rangle$ by which atoms scatter *back* into the condensate. The square of the matrix element M_2 for this process is $|C|^2 S(q) N_q n_{k-q} (N_0 + 1)(n_k + 1)$. The *net* rate W_+ of scattering atoms from the condensate into the quasi-particle mode \mathbf{q} is the difference of the two partial rates $W_+ = W_1 - W_2$. Assuming $N_0 \gg 1$ (i.e., $N_0 + 1 \approx N_0$), we obtain for the net rate

$$W_+ = \frac{2\pi}{\hbar} |C|^2 S(q) N_0 [n_k (N_q + n_{k-q} + 1) - N_q n_{k-q}] \delta(E_k - E_{k-q} - \hbar\omega_q^B). \tag{7}$$

For large n_k (e.g. a laser beam illuminating the condensate) the term $N_q n_{k-q}$ can be neglected, and the dominant bosonic stimulation term $(N_q + n_{k-q} + 1)$ is approximately $(\tilde{N} + 1)$ with $\tilde{N} = \max(N_q, n_{k-q})$. This illustrates that there is no bosonic stimulation of the net rate by the *least* populated final state. With the dynamic structure factor $S(\mathbf{q}, \omega) = S(q) \delta(\omega - \omega_q^B)$ Eq. 7 simplifies to

$$W_+ = \frac{2\pi}{\hbar^2} |C|^2 n_k S(\mathbf{q}, (E_k - E_{k-q})/\hbar) N_0 (N_q + n_{k-q} + 1). \tag{8}$$

The rate W_+ in Eq. 7 is the rate for the Stokes process where $E_k > E_{k-q}$. Momentum transfer $\hbar\mathbf{q}$ to the condensate is also possible as an anti-Stokes process where a quasi-particle with momentum $-\hbar\mathbf{q}$ is scattered into the condensate, and the scattered particle *gains* energy. The net rate W_- for this process is obtained in an analogous way as

$$W_- = \frac{2\pi}{\hbar} |C|^2 S(q) N_0 [n_k (N_{-q} - n_{k-q}) - (N_{-q} + 1) n_{k-q}] \delta(E_k - E_{k-q} + \hbar\omega_q^B). \tag{9}$$

The net scattering rates of Eqs. 7 and 9 involve the product of three terms.

- The static structure factor $S(q)$ represents the squared matrix element for the condensate to absorb momentum $\hbar\mathbf{q}$.
- The δ function denotes the density of final states.
- The bosonic stimulation term represents stimulation by the occupation in the final state either of the scattering particles or the condensate.

The interplay of these three terms is responsible for the enhancement and suppression of physical processes in a condensate. The properties of the condensate as an intriguing many-body system are reflected in the structure factor. In Sect. II, we discuss its measurement through stimulated light scattering. The density of states is responsible for superfluidity because it vanishes for initial velocities of the incident particles which are smaller than the Landau critical velocity (Sects. IV and V). Finally, bosonic stimulation by the occupancy N_q of final states was responsible for superradiance, matter wave amplification and optical amplification in a condensate (Sects. VII and VIII).

Sects. IX and X broaden the above discussion. In Sect. IX we show that there is a major difference how the condensate affects light scattering and spontaneous emission, i.e., spontaneous emission can probe properties of the condensate beyond the structure factor. Eq. 7 seems to imply that enhancement of a process requires macroscopic population of a quantum state, i.e., bosonic quantum degeneracy. The discussion on matter wave amplification for fermions in Sect. X shows that this is not the case, and that collective enhancement is possible even for fermions when they are prepared in a cooperative state.

II. DETERMINATION OF THE STATIC STRUCTURE FACTOR BY BRAGG SPECTROSCOPY

The matrix element or the structure factor in Eqs. 7 and 9 can be directly determined experimentally by light scattering. The density of states (the δ function in Eq. 7) does not restrict the scattering since the photon energy is much higher than the quasi-particle energy. As a result, photons can be scattered into the full solid angle and provide the necessary recoil energy of the atom by a small change ($\approx 10^{-9}$) in the frequency of the scattered photon.

When the light scattering is stimulated by a second laser beam, the momentum transfer $\hbar q$ is determined by the angle θ between the two laser beams: $\hbar q = 2\hbar k \sin(\theta/2)$. By varying the angle, one can probe both the phonon and free particle regime of the Bogoliubov quasiparticles (Fig. 1). Fig. 2 illustrates our experimental method for probing the response of a condensate at large momentum transfer. Counter-propagating laser beams were incident perpendicular to the long axis of the cigar-shaped condensate, which contained several million sodium atoms in the $F = 1, m_F = -1$ state [19]. After the momentum transfer, the condensate was allowed to freely expand, allowing scattered atoms to separate spatially from the unscattered atoms, as shown in the figure.

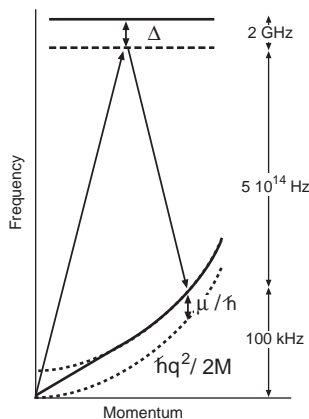


FIG. 1. Energy level diagram for Bragg spectroscopy. The solid line represents the energy of an atom at momentum $\hbar q$, which is given by the Bogoliubov dispersion relation for a homogeneous weakly-interacting Bose-Einstein condensate (Eq. 14). Excitations can be created optically by stimulated light scattering using two laser beams which are both far detuned (about 2 GHz) from the atomic resonance. Momentum and energy are provided by absorption of one photon to a virtual excited level, followed by stimulated emission of a second, lower energy photon. For small momenta $\hbar q$, such that $\hbar q \ll M c_s$ the dispersion relation is phonon-like (linear). Here M is the mass, and c_s is the speed of sound which is related to the interaction energy μ by $\mu = M c_s^2$. For large momenta $\hbar q \gg M c_s$ the dispersion relation is particle-like (quadratic) offset from the energy of a free-particle excitation by a mean-field shift of μ (≈ 5 kHz for our experiments).

For strong laser pulses and short times, the atoms undergo Rabi oscillations between the initial state and the recoil state (see Sec. VIII). For longer times, we can use rate equations (Eqs. 7 and 9), and obtain the rate W of transferring photons from one beam to the other as

$$W/N_0 = (W_+ + W_-)/N_0 = 2\pi(\Omega_R/2)^2 S(q) [\delta(\omega - \omega_q^B) - \delta(\omega + \omega_q^B)]. \quad (10)$$

The two laser beams have wavevectors \mathbf{k} and $\mathbf{k} - \mathbf{q}$ and a difference frequency ω . The two-photon Rabi frequency Ω_R is given by $(\hbar\Omega_R/2)^2 = |C|^2 n_k n_{k-q}$ (see Sec. VI).

When ω is scanned the “spectrum” of a condensate consists of two peaks at $\pm\omega_q^B$ (Fig. 3). The strength (or integral) of each peak corresponds to $S(q)$. We refer to this method as Bragg spectroscopy since the basic process is Bragg scattering of atoms from an optical standing wave. A full account of this method and the underlying theory was given in our Les Houches notes [10] (see also [15,20,21]).

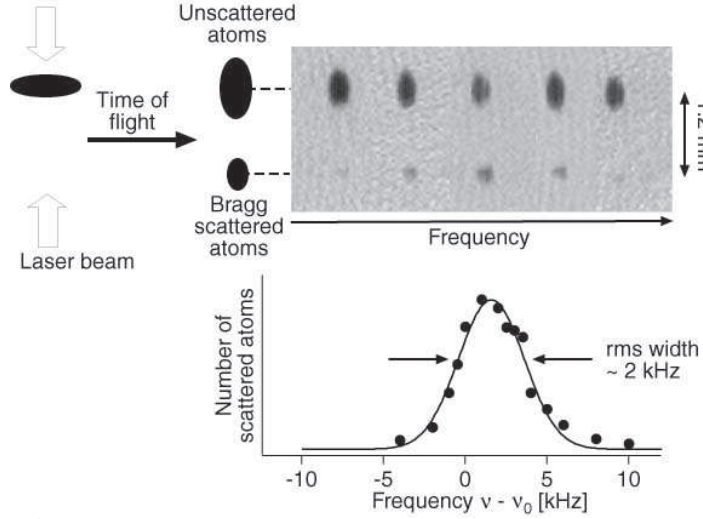


FIG. 2. Bragg spectroscopy. Atoms were stimulated by two counter-propagating laser beams to absorb a photon from one beam and emit it into the other beam, resulting in momentum transfer to the atoms, as observed in ballistic expansion after 20 ms time of flight. The number of scattered atoms showed a narrow resonance when the difference frequency ν between the two laser beams was varied around the recoil frequency ν_0 of the atoms.

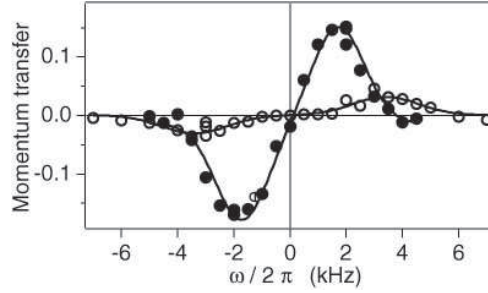


FIG. 3. Probing $S(q)$ by Bragg spectroscopy. Momentum transfer per particle, in units of $\hbar q$, is shown vs. the frequency difference $\omega/2\pi$ between the two Bragg beams. The two spectra were taken at different atomic densities. The open symbols represent the phonon excitation spectrum for a trapped condensate (at a chemical potential $\mu/\hbar = 9.2$ kHz, much larger than the free recoil shift of ≈ 1.4 kHz). Closed symbols show the free-particle response of a twenty-three times more dilute (ballistically expanded) cloud. Lines are fits to the difference of two Gaussian line shapes representing excitation in the forward and backward directions. See Refs. [15,10] for more details. Figure is taken from Ref. [15].

We observed that the scattering rate was strongly suppressed when the momentum transfer $\hbar q$ became smaller than the speed of sound c_s in the condensate (times the atomic mass M), i.e., when the light scattering excited a phonon and not a free particle. These observations are in agreement with the Bogoliubov theory, which obtains the elementary excitations or Bogoliubov quasiparticles as eigenstates of the Hamiltonian

$$\mathcal{H} = \sum_k \frac{\hbar^2 k^2}{2M} \hat{a}_k^\dagger \hat{a}_k + C \sum_{k,l,m,n} \hat{a}_l^\dagger \hat{a}_n^\dagger \hat{a}_k \hat{a}_m \delta_{l+n-k-m}. \quad (11)$$

The constant C can be expressed by the scattering length a as

$$C = \frac{2\pi\hbar^2 a}{MV} \quad (12)$$

where V is the condensate volume. The structure factor $S(q)$ (Eq. 4) is the norm of the state vector $\hat{\rho}(\mathbf{q})^\dagger |g\rangle / \sqrt{N}$ with the atomic density operator $\hat{\rho}(\mathbf{q})^\dagger = \sum_m \hat{a}_{m+q}^\dagger \hat{a}_m$. Only terms involving the zero-momentum state $m = 0$ yield significant contributions. Thus $S(q)$ is the norm of the vector

$$|e\rangle \approx \frac{(\hat{a}_q^\dagger \hat{a}_0 + \hat{a}_0^\dagger \hat{a}_{-q}) |g\rangle}{\sqrt{N}} \approx (\hat{a}_q^\dagger + \hat{a}_{-q}) |g\rangle = |e^+\rangle + |e^-\rangle \quad (13)$$

where we have replaced \hat{a}_0^\dagger and \hat{a}_0 by \sqrt{N} following the usual Bogoliubov formalism [3].

To calculate the norm of $|e\rangle$ explicitly, we transform to Bogoliubov operators $\hat{b}_q^\dagger = u_q \hat{a}_q^\dagger + v_q \hat{a}_{-q}$, where $u_q = \cosh \phi_q$, $v_q = \sinh \phi_q$ and $\tanh 2\phi_q = \mu/(\hbar\omega_q^0 + \mu)$ where $\hbar\omega_q^0 = \hbar^2 q^2/2M$ is the free-particle kinetic energy and μ is condensate's chemical potential. This yields $S(q) = (u_q - v_q)^2$. The static structure factor tends to $S(q) \rightarrow \hbar q/2mc_s$ and vanishes in the long wavelength limit, as required of a zero-temperature system with finite compressibility [22]. The speed of sound c_s is related to the chemical potential μ by $\mu = Mc_s^2$. The resonances in the Bragg spectrum occur at the energies $\hbar\omega_q^B$ of quasi-particles created by \hat{b}_q^\dagger

$$\hbar\omega_q^B = \sqrt{\hbar\omega_q^0(\hbar\omega_q^0 + 2\mu)}. \quad (14)$$

In our experiments we have observed the suppression of Bragg scattering at small angles. This implies an overall suppression of Rayleigh scattering which will be more pronounced when the speed of sound becomes comparable or larger than the recoil velocity. By integrating the static structure factor $S(q)$ over all possible scattering angles and accounting for the dipolar emission pattern, we find that Rayleigh scattering from a BEC is suppressed by a factor [15]

$$F_{\text{Bose}}^{\text{scatt}} = \frac{k_s}{\sqrt{k_s^2 + k_L^2}} \left(\frac{15}{8} \frac{k_s^5}{k_L^5} + \frac{23}{8} \frac{k_s^3}{k_L^3} + 2 \frac{k_s}{k_L} + \frac{k_L}{k_s} \right) - \left(\frac{15}{8} \frac{k_s^6}{k_L^6} + \frac{9}{4} \frac{k_s^4}{k_L^4} + \frac{3}{2} \frac{k_s^2}{k_L^2} \right) \tanh^{-1} \left(\frac{k_L}{\sqrt{k_s^2 + k_L^2}} \right). \quad (15)$$

where $\hbar k_L$ is the incident photon momentum and $\hbar k_s = Mc_s$ is the momentum of an atom moving at the speed of sound.

The long-wavelength suppression of $S(q)$ reveals a remarkable many-body effect. For free particles, the matrix element for momentum transfer is always 1, which reflects the fact that the operator $\exp(i\mathbf{q} \cdot \mathbf{r})$ connects an initial state with momentum \mathbf{p} to a state with momentum $\mathbf{p} + \hbar\mathbf{q}$ with unity overlap. For an interacting Bose-Einstein condensate, this overlap vanishes in the long-wavelength limit. As we have discussed in previous publications [15,10], this suppression of momentum transfer is due to a destructive interference between the two pathways for a condensate to absorb momentum $\hbar\mathbf{q}$ and create a quasi-particle: one pathway annihilates an admixture with momentum $-\hbar\mathbf{q}$, the other creates an admixture at momentum $+\hbar\mathbf{q}$.

The leading terms in stimulated light scattering do not depend on temperature. The rates W_+ and W_- (Eqs. 7 and 9) are independent of the thermally excited population of quasiparticles N_q and N_{-q} in the limit of large $n_k, n_{k-q} \gg N_{\pm q}$, i.e., when the scattering is stimulated by a second laser beam. For spontaneous scattering ($n_{k-q} = 0$), one obtains for the total scattering rate W instead of Eq. 10

$$W/N_0 = \frac{2\pi}{\hbar^2} |C|^2 S(q) n_k [(1 + N_q)(\delta(\omega - \omega_q^B) + N_{-q}\delta(\omega + \omega_q^B))]. \quad (16)$$

Absorption of and bosonic stimulation by thermally excited quasi-particles become important when the temperature is comparable to or larger than the quasi-particle energy $\hbar\omega_q^B$. Eq. 16 is proportional to the temperature dependent dynamic structure factor $S_T(\mathbf{q}, \omega)$ [23].

III. ATOMIC COLLISIONS IN A BOSE-EINSTEIN CONDENSATE

Before we discuss the analogies and differences between the scattering of light and massive particles, we make general remarks on particle scattering. We raise the question under what conditions can two matter waves penetrate each other without scattering. This includes the question what happens when two atom laser beams cross each other.

As we have seen in Sect. I, the scattering rate is proportional to the structure factor $S(\mathbf{q})$, which is a measure of the density-density correlations at wavevector \mathbf{q} associated with the momentum transfer. It consists of two parts, one reflects the average atomic density $\tilde{\rho}(\mathbf{q}) = \langle g|\hat{\rho}(\mathbf{q})|g\rangle$ and the other one the fluctuations $\delta\hat{\rho}(\mathbf{q}) = \hat{\rho}(\mathbf{q}) - \tilde{\rho}(\mathbf{q})$ (see also Eq. 95).

$$S(\mathbf{q}) = \frac{1}{N} \langle g|(\tilde{\rho}(\mathbf{q}) + \delta\hat{\rho}(\mathbf{q}))(\tilde{\rho}^*(\mathbf{q}) + \delta\hat{\rho}^\dagger(\mathbf{q}))|g\rangle \quad (17)$$

$$= \frac{1}{N} (\tilde{\rho}(\mathbf{q})\tilde{\rho}^*(\mathbf{q}) + \langle g|\delta\hat{\rho}(\mathbf{q})\delta\hat{\rho}^\dagger(\mathbf{q})|g\rangle) \quad (18)$$

In a system without fluctuations ($\delta\hat{\rho}(\mathbf{q}) = 0$), there is only scattering when the stationary density modulation allows for a momentum transfer at wavevector \mathbf{q} ($\hat{\rho}(\mathbf{q}) \neq 0$) and the incident particles fulfil the Bragg condition. One well known example is X-ray scattering off a crystal lattice. Electrons in such a lattice form stationary Bloch waves (superpositions of plane waves and Bragg scattered plane waves) and propagate without attenuation. Scattering only occurs at irregularities of the lattice or thermal fluctuations.

A Bose-Einstein condensate might appear perfectly ordered. However, as we have seen in Sect. II, it has density fluctuation similar to the classical ideal gas. The structure factor only differs from an ideal gas when the momentum transfer is comparable or less than the speed of sound (times the mass M). In the case of electromagnetic waves, these density fluctuation cause Rayleigh scattering. In close analogy, if a matter wave propagates through a condensate, there will be elastic scattering. On length scales larger than the healing length, the condensate has reduced density fluctuations, and we have seen that electromagnetic radiation of sufficiently long wavelength can propagate with only little scattering (Eq. 15). In the next section, we will find the equivalent result for long wavelength matter waves, but also a new effect, namely the complete suppression of scattering for velocities below the Landau critical velocity.

The scattering between two Bose-Einstein condensates can be nicely demonstrated by creating two condensates in a magnetic trap, one sitting at the bottom, the other one held up in the trapping potential by a blue-detuned light sheet which forms a repulsive potential for atoms. This initial situation was created by splitting a condensate into two halves using a light sheet [24] and then shifting the center of the magnetic trap by applying a magnetic field gradient. When the light sheet was switched off, one condensate accelerated and slammed into the other. The violent collision was observed *in situ* by phase contrast imaging and also analyzed by absorption imaging after ballistic expansion (Fig. 4).

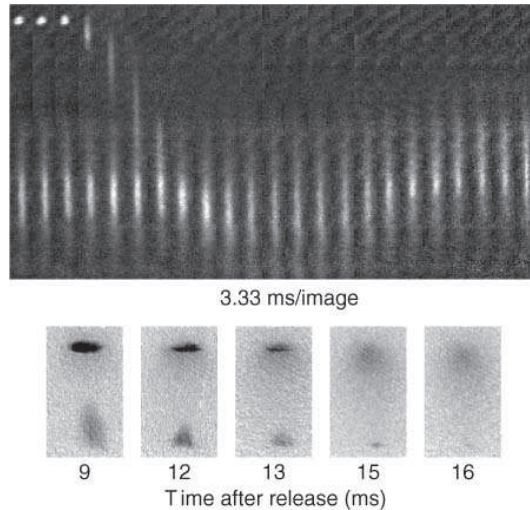


FIG. 4. Collisions between two condensates. One condensate was held up in the magnetic trapping potential by a blue-detuned light sheet and suddenly released. A series of phase-contrast images (upper part) and time-of-flight absorption images display the collision. The phase contrast pictures show the spreading of the upper condensate during acceleration, its collision, and merging with the stationary cloud. The time-of-flight pictures represent the velocity distribution. Before the scattering event, there were two distinct peaks representing the accelerated and the stationary condensate. After the collision, only one cloud was left which was heated up by the collision.



FIG. 5. Observation of elastic collisions between the condensate (lower black dot) and Bragg diffracted atoms (upper spot). The image is taken after a time-of-flight of 30 ms, and shows the velocity distribution after the collision. The products of the collision are distributed over a sphere in momentum space leading to the observed s -wave halo. The height of the image is 3.2 mm.

The method shown in Fig. 4 suffers from a large velocity spread of the incident condensate. A narrower velocity distribution can be achieved by Bragg scattering. With counter-propagating laser beams, we transferred two photon recoil momenta to some of the atoms. After the recoiling atoms had traversed the condensate the velocity distribution was probed in time-of-flight imaging and showed the characteristic s -wave halo (Fig. 5).

Such collisions between indistinguishable atoms of mass M are described by the interaction Hamiltonian in Eq. 11. This Hamiltonian is not only responsible for the interactions between two condensates, but also for the mean-field energy of a single condensate ($C\hat{a}_0^\dagger\hat{a}_0^\dagger\hat{a}_0\hat{a}_0$), pair correlations and quantum depletion ($C\sum_q\hat{a}_q^\dagger\hat{a}_{-q}^\dagger\hat{a}_0\hat{a}_0$) and the damping of collective excitations where a quasi-particle in mode k decays into two other excitations (Beliaev damping, $2C\sum_{l,n}\hat{a}_n^\dagger\hat{a}_l^\dagger\hat{a}_k\hat{a}_0\delta_{l+n-k-0}$) or promotes an existing quasi-particle in mode l to higher energy (Landau damping, $4C\sum_{k,n}\hat{a}_0^\dagger\hat{a}_n^\dagger\hat{a}_l\hat{a}_k\delta_{0+n-l-k}$).

Several papers discussed the outcoupling of atoms in mode k from a condensate at rest (mode 0) and only considered the term $2C\hat{a}_k^\dagger\hat{a}_0^\dagger\hat{a}_0\hat{a}_k$ which represents the mean-field repulsion between the two matter waves (see, for example, [25,26]). This term leads to a distortion of the outcoupled beam. However, this two-mode approximation neglects the scattering into the empty modes, described by

$$\mathcal{H}' = 2C \sum_{l,n} \hat{a}_l^\dagger \hat{a}_n^\dagger \hat{a}_k \hat{a}_0 \delta_{l+n-k-0} \quad (19)$$

In the following we want to show that this interaction leads to a scattering rate for particles in mode k

$$W_{\text{tot}} = n_0 \sigma v \quad (20)$$

with the condensate density $n_0 = N_0/V$, the cross-section $\sigma = 8\pi a^2$ and the relative velocity $v = \hbar k/M$. Eq. 20 therefore describes not only classical particles which collide with a cross-section σ , but also the quantum mechanical interaction between two matter waves.

We assume that the incident velocity is much larger than the speed of sound $v \gg c_s$. Therefore, there is no distinction between free particles and quasi-particles. In the center-of-mass frame the relevant terms in the Hamiltonian (Eq. 19) are

$$\mathcal{H}' = 4C \sum_q' \hat{a}_q^\dagger \hat{a}_{-q}^\dagger \hat{a}_{k/2} \hat{a}_{-k/2}, \quad (21)$$

where the prime indicates summation over one hemisphere. The additional factor of 2 (compared to Eq. 19) accounts for the fact that the final state $(\mathbf{q}, -\mathbf{q})$ appears twice in the summation (as $\mathbf{q}, -\mathbf{q}$ and $-\mathbf{q}, \mathbf{q}$, we only count the number of states in one hemisphere). Considering the collision of one particle with momentum $\hbar\mathbf{k}$ with a pure condensate, we write the initial and final states $|N_{k/2}, N_q; N_{-k/2}, N_{-q}\rangle$ (see Eq. 2) as

$$\begin{aligned} |i\rangle &= |1, 0; N_0, 0\rangle \\ |f\rangle &= |0, 1; N_0 - 1, 1\rangle. \end{aligned} \quad (22)$$

The square of the matrix element for the Hamiltonian (Eq. 21) between those two states is $|M|^2 = 16|C|^2 N_0$. From Eq. 6 (Fermi's golden rule) the scattering rate follows as

$$\begin{aligned} W_{\text{tot}} &= \frac{2\pi}{\hbar} \sum_f |M|^2 \delta(E_f - E_i) \\ &= \frac{2\pi}{\hbar} |M|^2 \int \left(\frac{d\rho}{dE_f} \right) \delta(E_f - E_i) dE_f \end{aligned} \quad (23)$$

with the final and initial energies $E_f = 2 \times \hbar^2 q^2 / 2M$, $E_i = 2 \times \hbar^2 (k/2)^2 / 2M$. The density of final states $d\rho/dE_f$ is equal to half the density of single particle states evaluated at $E_{\text{single}} = E_f/2$. The density of single particle states at energy E is

$$\frac{d\rho}{dE} = \frac{1}{2} \times \frac{V}{(2\pi)^3} 2\pi \left(\frac{2M}{\hbar^2} \right)^{3/2} E^{1/2} \quad (24)$$

The additional factor of (1/2) comes from the fact that for pairs of indistinguishable particles, we only count the number of states in one hemisphere.

Thus, the density of final states is

$$\frac{d\rho}{dE_f} = \frac{1}{2} \frac{d\rho}{dE} \Big|_{E=E_f/2} = \frac{V}{(2\pi)^3} \frac{\pi}{2} \left(\frac{2M}{\hbar^2} \right)^{3/2} (E_f/2)^{1/2} \quad (25)$$

Substituting Eq. 25 into Eq. 23 gives $q = k/2$ and finally Eq. 20.

In the center-of-mass frame, the scattered particles occupy a shell in momentum space at $q = k/2$ (see Fig. 5). The quantum-mechanical origin of the relative velocity v in Eq. 20 is the density of final states which is proportional to $\sqrt{E} \propto v$. The scattering of atoms into empty modes is not described by the Gross-Pitaevskii equation (which only describes macroscopically occupied modes), but can be accounted for by introducing a complex scattering length into the Gross-Pitaevskii equation [27].

For the scattering of impurity atoms with the same mass as the condensate atoms the constant C in Eq. 1 is

$$C = \frac{4\pi\hbar^2 a}{MV}, \quad (26)$$

or more generally $C = 2\pi\hbar^2 a/\mu V$ where μ is the reduced mass and a is now the scattering length for collisions between condensate and impurity atoms. The factor of two difference between Eqs. 26 and 12 is necessary to avoid double counting of identical atom pairs. If we repeat the above derivation for impurity atoms we obtain a cross-section of $\sigma = 4\pi a^2$, whereas the cross-section for indistinguishable particles is twice as large. This reflects several factors of 2 and 4: The factor of (1/2) in the constant C ; the factor of 4 in Eq. 21 which expresses that each initial and final state appears four times in Eq. 11; the momentum integral for indistinguishable particles extends only over the hemisphere whereas distinguishable particles have twice the number of possible final states.

We used images like Fig. 5 (for indistinguishable atoms) and Fig. 8a for impurity atoms (see following section) to determine the collision cross sections. The cross-section for indistinguishable atoms was found to be 2.1 ± 0.3 times larger than the one for impurities in agreement with the expected factor of two [11].

IV. SUPPRESSION OF IMPURITY COLLISIONS

The key difference between the scattering of light and massive particles (or impurities) is their energy-momentum dispersion relation. The dispersion relation for impurities is $E_k = (\hbar k)^2/2M$, whereas for light, $E_k = \hbar k c$ with c denoting the speed of light. This difference is responsible for the complete suppression of impurity scattering at low velocities. For simplicity, we assume equal mass M for the impurity and condensate atoms.

Energy-momentum conservation, the δ function in Eq. 7, requires $E_k - E_{k-q} = \hbar\omega_q^B$. For impurity particles, the l.h.s. is always less than $v\hbar q$, where $v = \hbar k/M$ is the initial velocity of the impurities. Thus, collisions with the condensate are only possible, if this maximum energy transfer is sufficient to excite a quasi-particle, i.e., $v > \min(\omega_q^B/q) = v_L$, where v_L is the Landau critical velocity [28] for superfluidity below which no dissipation occurs because the density of final states vanishes.

For the excitation spectrum of the condensate (Eq. 14), the Landau velocity is the Bogoliubov speed of sound $v_L = c_s = \sqrt{\mu/M}$. Impurity particles moving below this speed cannot dissipate energy in collisions. In contrast, for photons, $dE_k/d(\hbar k) = c \gg c_s$, and scattering is always possible.

In the perturbative limit (no stimulation by the final occupation), the total rate of scattering W_{tot} is given by integrating Eq. 7 over all possible momentum transfers. In the derivation above for large incident velocities we absorbed the angular integral in the density of states since the scattering in the center-of-mass frame is isotropic. Now it is necessary to consider the scattering angles explicitly. Furthermore, we stay in the frame where the condensate is at rest. Straightforward transformations lead to

$$\begin{aligned} W_{\text{tot}} &= \frac{2\pi|C|^2}{\hbar^2} N_0 \sum_{\mathbf{q}} S(q) \delta \left(\frac{\hbar\mathbf{k} \cdot \mathbf{q}}{M} - \frac{\hbar q^2}{2M} - \omega_q^B \right) \\ &= (N_0/V) \left(\frac{2\hbar a}{M} \right)^2 \int dq d\Omega q^2 S(q) \delta \left(\frac{\hbar k q \cos \theta}{M} - \frac{\hbar q^2}{2M} - \omega_q^B \right) \end{aligned}$$

$$\begin{aligned}
&= 2\pi(N_0/V) \left(\frac{2\hbar a}{M}\right)^2 \frac{1}{v} \int_0^Q dq qS(q) \\
&= (N_0/V) \sigma(\eta) v,
\end{aligned} \tag{27}$$

where $\hbar Q = Mv(1 - 1/\eta^2)$ is the maximum possible momentum transfer, and $\eta = v/c_s$ must be larger than 1. The collision cross-section is $\sigma(\eta) = \sigma_0 F(\eta)$ where $\sigma_0 = 4\pi a^2$. For $\eta < 1$, $F(\eta) = 0$ and for $\eta > 1$, $F(\eta) = 1 - 1/\eta^4 - \log(\eta^4)/\eta^2$.

The suppression factor $F(\eta)$ is determined by two factors: the phase space restriction due to the δ function in Eq. 27, and additional suppression at low momentum transfers by the structure factor of the condensate. For decreasing velocity, the possible scattering angles θ become restricted to a forward scattering cone ($\theta < \arccos(1/\eta)$), which shrinks to zero solid angle at the Landau critical velocity (Fig. 6). This reflects that near the Landau velocity, the scattered particle has “difficulties” to provide enough energy per momentum to create phonons. The maximum energy transfer occurs when the momentum transfer is collinear with the incident velocity, i.e., for small angle scattering angles. A graph of the suppression factor as function of impurity velocity is shown in Fig. 7.

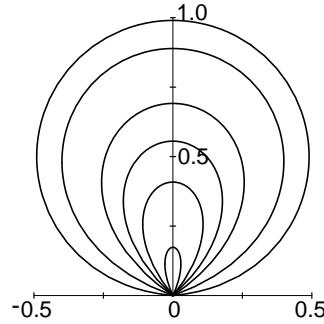


FIG. 6. Momentum transfer in collisions. The polar diagram shows the momentum transfer (in units of the initial momentum) vs. scattering angle θ for different values of $\eta = v/c_s$ (10, 3, 1.8, 1.5, 1.3, 1.1). As the impurity velocity approaches the speed of sound ($\eta \rightarrow 1$), the scattering cone shrinks to zero solid angle.

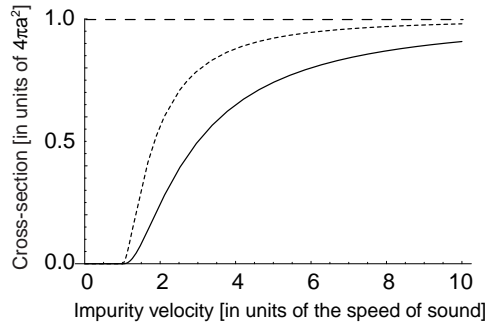


FIG. 7. Suppression of collisions. Shown is the suppression factor as a function of the impurity velocity (normalized by the speed of sound c_s , solid line). The dotted line represents the suppression due to phase-space restriction alone (i.e., setting the structure factor $S(q) = 1$).

Experimentally, the Landau critical velocity can usually only be observed by moving *microscopic* particles through the superfluid which do not create a macroscopic flow pattern. Studies of superfluidity with microscopic objects were pursued in liquid ^4He by dragging negative ions through pressurized ^4He [29,30], and by scattering ^3He atoms off superfluid ^4He droplets [31].

To study the effects of impurities interacting with the condensate, we created microscopic impurity atoms using a stimulated Raman process which transferred a small fraction of the condensate atoms in the $|F = 1, m_F = -1\rangle$ hyperfine state into an untrapped hyperfine state $|F = 1, m_F = 0\rangle$ with a well-defined initial velocity [32]. The initial velocity could be adjusted between zero and two single-photon recoil velocities by varying the angle between the two

Raman beams. As these impurities traversed the condensate, they collided with the stationary condensate, resulting in a redistribution of the impurity momenta which was detected by a time-of-flight analysis [11] (Fig. 8).

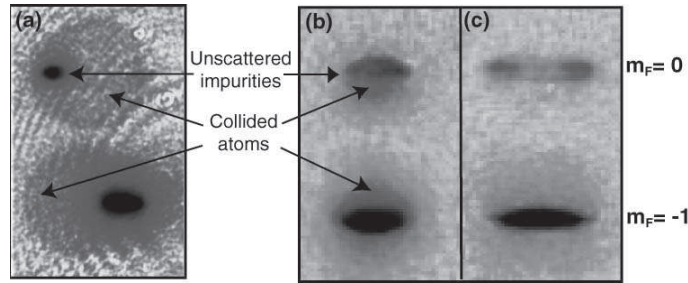


FIG. 8. Observation of elastic collisions between the condensate and impurity atoms. (a) Impurities traveling at 6 cm/s along the radial axis (to the left in images) were scattered into an s -wave halo. Absorption image after 50 ms of time-of-flight shows the velocity distribution after collisions between the condensate (bottom) and the outcoupled $m_F = 0$ atoms (top), spatially separated by a Stern-Gerlach type magnetic field gradient. The collisional products are distributed over a sphere in momentum space. The image is 4.5×7.2 mm. (b) Similar image as (a) shows the collisional products (arrow) for impurity atoms (top) traveling at 7 mm/s along the condensate axis (upward in image). For this image, $v_g/c_s = 2.7$ (see text). Collisions are visible below the unscattered impurities. (c) Similar image as (b) with $v_g/c_s = 1.6$. Collisions are suppressed. The momentum distribution of the outcoupled atoms was distorted by mean-field repulsion. The images are 2.0×4.0 mm. Figure is taken from Ref. [11].

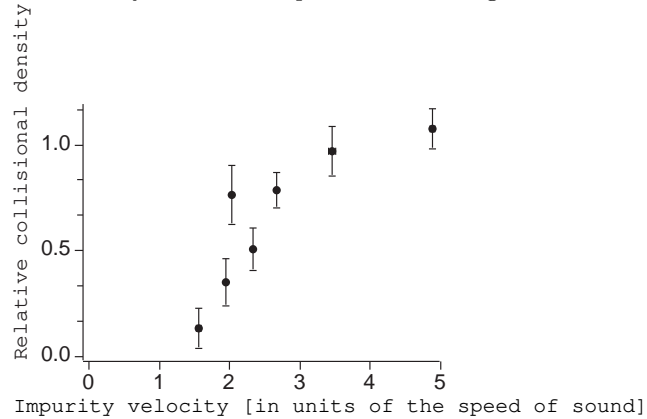


FIG. 9. Onset of superfluid suppression of collisions. Shown is the observed collisional density normalized to the predicted one in the limit of high velocities as a function of $\bar{\eta} = v_g/c_s$, which is a measure of the impurity velocity in units of the condensate's speed of sound. The error bars represent the statistical uncertainty. Data is taken from Ref. [11].

To probe for the suppression of collisions, the impurity velocity has to be varied around the speed of sound. For that, we produced impurity atoms at low velocities (7 mm/s) and varied the speed of sound by changing the condensate density. The small axial velocity imparted by Raman scattering allowed us to identify products of elastic collisions in time-of-flight images (Fig. 8b, c) since collisions with the stationary condensate redistributed the impurity atoms toward lower axial velocities. However, the impurity velocity was predominantly determined by the gravitational acceleration g , which imparted an average velocity of $v_g = \sqrt{gt_z}$ where l_z is the Thomas-Fermi diameter of the condensate in the z -direction. Thus, the effect of superfluidity on impurity scattering depends primarily on the parameter $\bar{\eta} = v_g/c_s$ which is the ratio of the typical impurity velocity v_g to the speed of sound c_s at the center of the condensate.

A time-of-flight analysis of impurity scattering for the case of a low-density condensate (small c_s) and large condensate radius (large v_g) is shown in Fig. 8b. The effect of collisions is clearly visible with about 20% of the atoms scattered to lower axial velocities (below the unscattered impurities in the image). In contrast, in the case of tight confinement, the condensate density is higher (larger c_s) and its radius is smaller (smaller v_g), and the collision probability is greatly suppressed due to superfluidity (Figs. 8c and 9).

The bosonic stimulation factor in Eq. 7 becomes relevant if the final states are populated, either by scattering or thermally. We observed that the fraction of collided atoms increased with the number of outcoupled impurities (Fig. 10). For a large outcoupled fraction, population n_{k-q} and N_q is built up in the final states and stimulates further scattering. This collisional amplification is not directional, and is similar to the recently observed optical omnidirectional superfluorescence [33].

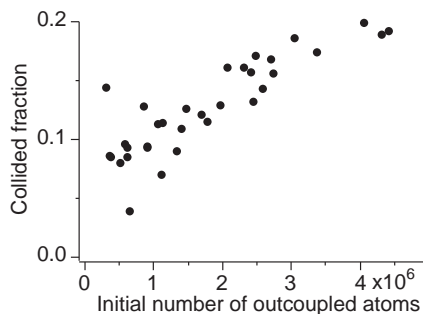


FIG. 10. Collective amplified elastic scattering in a Bose-Einstein condensate. Shown is the fraction of collided atoms vs. the number of outcoupled atoms. For this data, $v_g/c_s=4.9$ and the chemical potential was 1.8 kHz. Figure is taken from Ref. [11].

Gain of momentum and thus transfer of energy from the condensate to the impurity atoms is impossible at zero temperature, but may happen at finite temperature due to the presence of thermal excitations (the N_{-q} term in Eq. 9)². Thus finite temperature enhances the elastic cross-section by two effects: Absorption of quasi-particles (anti-Stokes process) and stimulation of momentum transfer by the final state population (Stokes process).

Fig. 11 shows the dramatic variation of the elastic scattering cross-section with temperature. However, the finite temperature did not affect our data in a major way: Due to gravitational acceleration we couldn't probe the velocity regime well below the Landau critical velocity where only thermally assisted collisions are possible. Furthermore, when we counted the number of collided atoms we had to use a background subtraction method where we subtracted the small signal of the energy gain collisions from the energy loss collisions (see Ref. [11] for details), thus cancelling most of the finite-temperature effects.

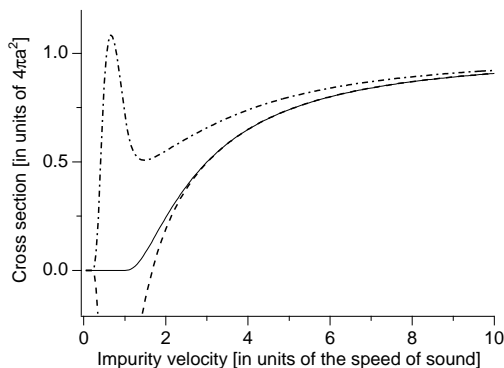


FIG. 11. Temperature dependent cross-section vs. impurity velocity. Shown is the cross-section at zero temperature (solid line) and at a finite temperature $kT = \mu$ which is typical for our experimental conditions (dash-dotted line). The finite temperature cross-section includes collisions involving thermally occupied quasi-particles where the impurities lose or gain energy. In the experiment, we measured the number of impurities which lost its energy minus the number which gained energy. Thus, the experimental measured cross-sections (Fig. 9) should be compared to $\sigma_{\text{coll,loss}} - \sigma_{\text{coll,gain}}$ (dashed line).

V. SUPPRESSION OF DISSIPATION FOR A MOVING MACROSCOPIC OBJECT

So far, we have discussed the suppression and enhancement of microscopic processes (light scattering and impurity collisions). The suppression of dissipation is even more dramatic on the macroscopic scale. The flow of liquid ^4He and the motion of macroscopic objects through it are frictionless below a critical velocity [34]. Recently, we have explored such frictionless flow in a gaseous BEC [12,13].

The microscopic and macroscopic cases bear many parallels. The onset of scattering or dissipation has two requirements: one needs final states which conserve energy and momentum, and an overlap matrix element which populates

²We are grateful to S. Stringari for pointing out the importance of finite-temperature effects.

these states. In the case of macroscopic flow, the first requirement leads to a critical velocity for vortex creation and the second requirement addresses the nucleation process of vortices.

The Landau criterion for superfluidity shows that excitations with momentum p and energy $E(p)$ are only possible when the relative velocity between the fluid and the walls or a macroscopic object exceeds the Landau critical velocity v_L which is given by $v_L = \min(E(p)/p)$ (see e.g. [2,34]). A similar criterion applied to vortex formation yields

$$v_c = \frac{E_{\text{vortex}}}{I_{\text{vortex}}} \sim \frac{\hbar}{MD} \ln\left(\frac{D}{\xi}\right) \quad (28)$$

where $I_{\text{vortex}} = \int p \, d^3r$ is the integrated momentum of the vortex ring or line pair, E_{vortex} is its total energy, D is the dimension of the container, and ξ the core radius of a vortex which in the case of dilute gases is the healing length $\xi = 1/\sqrt{8\pi\rho a}$. Ref. [34] derived Eq. 28 for vortex rings with a maximum radius D , Ref. [35] looked at pairs of line vortices at distance D . Feynman [36] found a similar result for superflow through a channel of diameter D .

An analogous result is obtained for a Bose condensed system placed under uniform rotation with angular velocity Ω . A vortex becomes energetically allowed when its energy E' in the rotating frame drops to zero,

$$E' = E - \Omega L = 0, \quad (29)$$

where E and L are the energy and angular momentum in the laboratory frame. This defines a critical *angular* velocity below which a vortex cannot be sustained due to conservation of angular momentum and energy [37]:

$$\Omega_c = \frac{E_{\text{vortex}}}{L_{\text{vortex}}} \sim \frac{\hbar}{MD^2} \ln\left(\frac{D}{\xi}\right). \quad (30)$$

The critical velocity at the wall of the rotating container, $v_c = D\Omega_c$, agrees with Eq. 28. However, Eqs. 28 and 30 only reflect the energy and momentum required to generate vortices, and do not take into account the nucleation process. If the scattering particle is macroscopic in size, the coupling is between the ground state and a state containing a vortex. Populating such a state requires nucleation of the vortex by the perturbing potential, which usually does not occur until higher velocities are reached than those predicted by Eqs. 28 and 30. The other option, the formation of the vortex by macroscopic quantum tunneling between the two states is an extremely slow process. In recent experiments in which a Bose condensate was placed in a rotating potential, the critical angular velocity for the formation of a single vortex was observed to be 1.6 times higher than the value given by Eq. 30 [38]. This discrepancy may be due to a nucleation barrier associated with the excitation of surface modes, as some authors have recently suggested [39,40].

To study frictionless flow in a Bose-condensate, we focused an argon ion laser beam (at 514 nm) onto the condensate, which repelled atoms from the focus. The laser beam was scanned back and forth along the axial direction of the condensate, creating a moving “hole” that simulated a macroscopic object. Rapid sequence phase-contrast imaging allowed us to directly measure the density profile of the superfluid around the moving laser beam.

For a weakly interacting Bose-condensed gas at density $\rho(\mathbf{r})$ and chemical potential $\mu(\mathbf{r})$, pressure is identical to the mean-field energy density $P = \mu(\mathbf{r})\rho(\mathbf{r})/2$ [7]. A drag force arises due to the pressure difference across the moving object. The chemical potential is given by $\mu(\mathbf{r}, t) = g\rho(\mathbf{r}, t)$, where $g = CV = 4\pi\hbar^2 a/M$ is the strength of two-body interactions. The drag force F is given by

$$F \simeq gS\rho\Delta\rho = S\mu\Delta\mu/g \quad (31)$$

where $\Delta\rho$ and $\Delta\mu$ are the differences in density and chemical potential across the stirring object, and S the surface area the macroscopic object presents to the condensate.

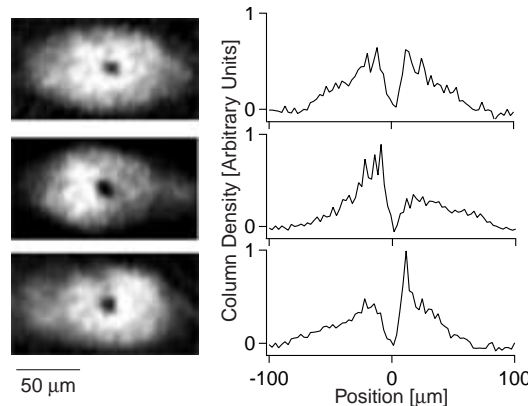


FIG. 12. Pressure difference across a laser beam moving through a condensate. On the left side *in situ* phase contrast images of the condensate are shown, strobed at each stirring half period: beam at rest (top); beam moving to the left (middle) and to the right (bottom). The profiles on the right are horizontal cuts through the center of the images. The stirring velocity and the maximum sound velocity were 3.0 mm/s and 6.5 mm/s respectively. Figure is taken from Ref. [13].

If the laser beam is stationary, or moves slowly enough to preserve the superfluid state of the condensate, there will be no gradient in the chemical potential across the laser focus, and therefore zero force according to Eq. 31. A drag force between the moving beam and the condensate is indicated by an instantaneous density distribution $\rho(\mathbf{r}, t)$ that is distorted asymmetrically with respect to the laser beam. Fig. 12 shows phase contrast images strobed at half the stirring period (where the laser beam is in the center of the condensate). A bow wave and stern wave form in front of and behind the moving laser beam, respectively. We define the asymmetry A as the relative difference between the peak column densities in front ($\bar{\rho}^f$) and behind ($\bar{\rho}^b$) the laser beam $A = 2(\bar{\rho}^f - \bar{\rho}^b)/(\bar{\rho}^f + \bar{\rho}^b)$. The asymmetry A is proportional to the drag force F .

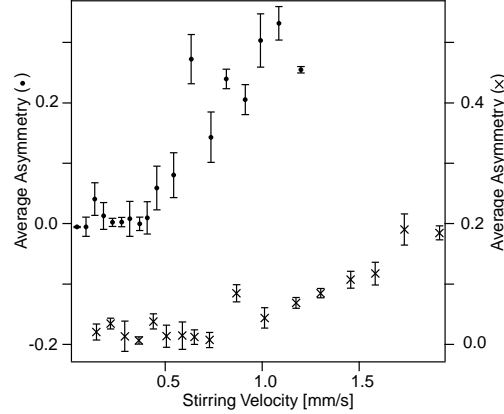


FIG. 13. Density dependence of the critical velocity. The onset of the drag force is shown for two different condensate densities, corresponding to maximum sound velocities of 4.8 mm/s (•, left axis) and 7.0 mm/s (x, right axis). The stirring amplitudes are 29 μm and 58 μm , respectively. The two vertical axes are offset for clarity. The bars represent statistical errors. Figure is taken from Ref. [13].

In Fig. 13 we show measurements of the asymmetry for two maximum densities ρ_0 of 9×10^{13} and $1.9 \times 10^{14} \text{ cm}^{-3}$. In each data set there is a threshold velocity v_c below which the drag force is negligible, and this threshold increases at higher density. Its value is close to $0.1 c_s$ for both data sets, where c_s is the sound velocity. Above this critical velocity, the drag force increases monotonically, with a larger slope at low density.

One can compare measurements of the asymmetry (proportional to the drag force \mathbf{F}) with the rate of energy transferred to the condensate, $\mathbf{F} \cdot \mathbf{v}$, using the calorimetric technique introduced in [12]. For this, the condensate was stirred for times between 100 ms and 8 s, in order to produce approximately the same final temperature. After the stirring beam was shut off, the cloud was allowed to equilibrate for 100 ms. Using ballistic expansion and absorption imaging, we determined the thermal fraction and thus the temperature and total energy.

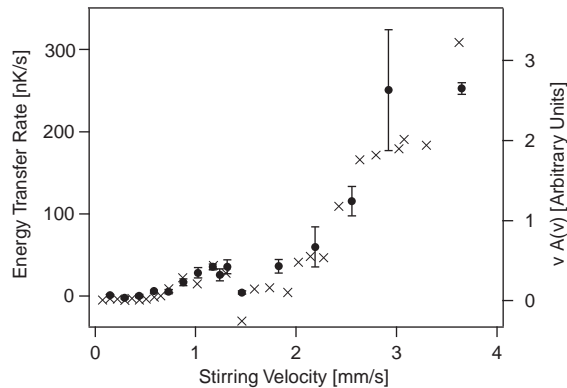


FIG. 14. Calorimetry of a condensate. The energy transfer rate during stirring (\bullet , left axis) was obtained from temperature measurements. The error bars reflect shot-to-shot variations in the temperature. The results are compared to the energy transfer rate $vA(v)$ obtained from asymmetry measurements of the flow field during the stirring (\times , right axis). Figure is taken from Ref. [13].

The calorimetric measurements can be compared with the drag force inferred from the asymmetric density distribution. Using Eq. 31, the energy transfer rate per atom is written in terms of the asymmetry as

$$\left. \frac{dE}{dt} \right|_{\text{asym}} \equiv \frac{\mathbf{F} \cdot \mathbf{v}}{N} \approx \frac{8}{15} \frac{\mu_0 \rho_0 l_z D}{N} vA(v) \quad (32)$$

where D is the diameter of the laser beam and l_z the Thomas Fermi diameter in the radial direction.

Fig. 14 shows that the calorimetric and the drag force measurements are in remarkable agreement over the entire velocity range up to a single scale factor for $vA(v)$, demonstrating the consistency between the two methods. For the parameters of our experiment ($D \simeq 10\mu\text{m}$, $\rho_0 = 1.3 \times 10^{14} \text{ cm}^{-3}$, $l_z = 66\mu\text{m}$, $N = 1.8 \cdot 10^7$) the overall heating rate predicted by Eq. 32 is 2.4 times larger than that obtained directly from calorimetry. Possible explanations for this difference are the inhomogeneous density profile or a breakdown of the quasi-static approximation embodied in Eqs. 31 and 32.

The observed critical velocity may be related to the formation of vortices. An estimate based on Eq. 28 for typical experimental parameters in sodium ($D = 10 \mu\text{m}$, peak density $\rho_0 = 1.5 \times 10^{14} \text{ cm}^{-3}$, $a = 2.75 \text{ nm}$) yields $v_c \simeq 1.0 \text{ mm/s}$, close to the experimental observations. However, Eq. 28 depends only weakly on the speed of sound, through the logarithmic dependence on the healing length ξ . In contrast, our measurements show an approximate proportionality to the sound velocity [13], suggesting that vortex nucleation determines the onset of dissipation.

Time-dependent simulations of the Gross-Pitaevskii equation show the formation of vortex line pairs above a critical velocity which is close to the observed value [41]. Several authors have emphasized the role of locally supersonic flow around the laser beam in the nucleation of vortices [41–43]. In one theoretical model [42], the vortices are emitted periodically at a rate that increases with velocity, and reduce the pressure gradient across the object. The predicted heating rate [42,44] is in rough agreement with the experimental results. Moreover, this model also predicts that the slope of the asymmetry vs. velocity should increase at lower density, in accord with our observations (Fig. 13).

The calorimetric measurements were extended to purely thermal clouds [45]. By accounting for the different geometries of the clouds, we could infer the effective energy transfer to an atom in a collision with the stirrer. For velocities well above the critical velocity we found almost equal energy transfer. This result fits well into the picture that the special properties of a condensate only show up in processes where little energy is transferred to the atoms.

VI. FOUR-WAVE MIXING OF LIGHT AND ATOMS

Our discussion on amplification of light and atoms in a BEC in the next section will reveal novel aspects of the coupling between light and atoms. In preparation for this, we want to present some general aspects of the scattering Hamiltonian in Eq. 1 applied to the scattering of photons from the condensate (the operators \hat{c}_l^\dagger , \hat{c}_k are now creation and annihilation operators for photons). The coupling can be regarded as four-wave mixing of two atomic fields and two electromagnetic fields.

When an atom is illuminated by two strong laser beams in a Λ configuration similar to Fig. 1, the electronically excited state can be adiabatically eliminated for sufficiently large detuning Δ . The coupling matrix element between the two atomic ground states is $\hbar\Omega_R/2$, where Ω_R is the two-photon Rabi frequency. This Rabi frequency can be expressed by the (complex) electric field strength $E_{1,2}$ of the two laser beams: $\Omega_R = \Omega_1\Omega_2 \cos\phi/2\Delta$, where $\Omega_{1,2} = E_{1,2}d/\hbar$ are the Rabi frequencies of the individual laser beams with the atomic dipole matrix element d . ϕ is the angle between the axes of polarization of the two laser beams. The two-photon Rabi frequency Ω_R can be rewritten as

$$\Omega_R = d^2 E_1 E_2 \cos\phi / 2\hbar^2 \Delta. \quad (33)$$

Using the Hamiltonian in Eq. 1, the coupling matrix element squared is $|C|^2 n_1 n_2$ where $n_{1,2}$ are the photon numbers in the two beams. The two-photon Rabi frequency Ω_R is given by

$$(\hbar\Omega_R/2)^2 = |C|^2 n_1 n_2. \quad (34)$$

Expressing the number n_1 of photons with angular frequency ω_0 in a volume V by the complex electric field strength E_1

$$n_1 = \epsilon_0 |E_1|^2 V / 2\hbar\omega_0, \quad (35)$$

and comparing to Eq. 33 we obtain for the coupling constant C between the two modes

$$C = \frac{\omega_0 d^2 \cos \phi}{2\epsilon_0 V \Delta}. \quad (36)$$

Another simple limit of the Hamiltonian in Eq. 1 is the situation when atoms are illuminated by a single laser beam in mode 1. Then the diagonal term $C \hat{c}_1^\dagger \hat{a}_0^\dagger \hat{c}_1 \hat{a}_0$ gives rise to the AC Stark shift. With the photon number n_1 , the AC Stark shift ΔE of an atom is $\Delta E = C n_1$. Using Eqs. 35 and 36 with $\cos \phi = 1$ one obtains the well known result, $\Delta E = d^2 E_1^2 / 4\hbar\Delta$.

Since the four-wave mixing Hamiltonian (Eq. 1) applies to interactions of a condensate both with light and atoms, we can draw analogies. The AC Stark shift corresponds to the mean field interaction between impurity atoms and the condensate. In Sec. III we saw how the scattering of atoms into empty modes gave rise to the usual elastic collision rate. Similarly, the scattering of photons into empty modes by the four-wave mixing Hamiltonian results in Rayleigh scattering which we want to discuss now in more detail.

Rayleigh scattering is described by Eq. 7. In the limit of weak scattering and for non-interacting atoms ($S(q) = 1$) one obtains

$$W_+ / N_0 = \frac{2\pi}{\hbar} |C|^2 n_1 \delta(E_k - E_{k-q} - \hbar\omega_q^0). \quad (37)$$

The scattering rate per solid angle $d\gamma_{\text{scatt}}/d\Omega$ is given by integrating this equation over all final states using the density of states per energy interval and solid angle

$$\frac{d\rho}{dE d\Omega} = \frac{V\omega_0^2}{(2\pi c)^3 \hbar}. \quad (38)$$

Using Eqs. 35, 36 one obtains

$$\frac{d\gamma_{\text{scatt}}}{d\Omega} = \frac{2\pi}{\hbar} |C|^2 n_1 \frac{d\rho}{dE d\Omega} = \frac{\omega_0^3 E_1^2 d^4 \cos^2 \phi}{32\pi^2 \hbar^3 c^3 \epsilon_0 \Delta^2}. \quad (39)$$

With the expression for the natural linewidth Γ

$$\Gamma = \frac{d^2 \omega_0^3}{3\pi \epsilon_0 \hbar c^3}, \quad (40)$$

this simplifies to

$$\frac{d\gamma_{\text{scatt}}}{d\Omega} = \frac{3 \cos^2 \phi}{8\pi} \frac{\Omega_1^2}{4\Delta^2} \Gamma = \frac{3 \sin^2 \theta}{8\pi} R, \quad (41)$$

where we have defined the Rayleigh rate R

$$R = \frac{\Omega_1^2}{4\Delta^2} \Gamma. \quad (42)$$

θ denotes the angle between the linear polarization of the incident light and the direction of the scattered light. For each scattering angle θ there are two polarizations of the scattered light. One is orthogonal to the incident polarization, thus $\cos \phi = 0$ in Eq. 36, and it doesn't contribute. The density of states in Eq. 38 was therefore defined for only one polarization. The other polarization is in the plane of the incident polarization and the scattering direction, thus $\cos \phi = \sin \theta$. R was defined in Eq. 42 in such a way that integration of Eq. 41 over the whole solid angle gives $\gamma_{\text{scatt}} = R$.

Below, we will need another useful expression for the two-photon Rabi frequency Ω_R . We use Eq. 34, assume that one laser beam is a weak probe beam with photon number n_p , express the photon number of the other (strong) beam by its Rayleigh scattering rate and obtain

$$\Omega_R^2 = 6\pi R\lambda^2 c n_p / V. \quad (43)$$

Four-wave mixing between atoms and light has two important limiting cases. In one case, atoms are diffracted by a standing wave of light, i.e., the atoms move in the AC Stark shift potential of two interfering light fields. In the other case, light is diffracted by a matter wave grating, a density modulation formed by two interfering matter waves.

In the first case, the AC Stark shift potential is proportional to $\sqrt{n_k n_l}$, where $n_{k,l}$ are the number of photons in the two laser beams. The diffraction efficiency is proportional to the square of the potential, and therefore, for N_q atoms in the incident mode, the scattering rate is proportional to $n_k n_l N_q$. In the latter case, the density modulation caused by the interference between N_k and N_l atoms is proportional to $\sqrt{N_k N_l}$. The scattering rate for light with n_q photons is then proportional to $N_k N_l n_q$. Applying this to a condensate with N_0 atoms illuminated with a (strong) laser beam with n_k photons, we see from Eq. 8 that for $N_q < n_{k-q}$ one has Bragg scattering, the scattering of atoms from a standing wave of light. This is usually realized by illuminating the atoms with two laser beams. For $N_q > n_{k-q}$ the physical picture is the diffraction of light by an atomic density modulation. It is this regime, which we have exploited for the amplification of atoms in a Bose-Einstein condensate (see Sect. VIII for a further discussion).

Generally, the optical (or atomic) gratings are moving. As a result, the diffracted atoms (or photons) have an energy different from that of the incident particles. However, one can always transform to a moving frame where the grating is stationary and there is no energy transfer in the scattering process. The frequency shift due to the moving grating can therefore be regarded as the Doppler shift related to the Galilean transformation between the two frames.

VII. SUPERRADIANCE AND MATTER WAVE AMPLIFICATION

Spontaneous light scattering can be stimulated when the atomic recoil state is already populated (the N_q term in Eq. 7). We have explored this process in our studies of superradiance [14], phase-coherent atom amplification [17], and optical amplification [18].

In all these experiments, the condensate was illuminated with a laser beam (mode k , also called the “dressing beam”). A condensate atom scatters a photon from the laser beam into another mode and receives the corresponding recoil momentum and energy. Injection of atoms turns this *spontaneous* process into a *stimulated* process and realizes an amplifier for atoms. The injected atoms interfere with the condensate at rest and form a matter wave grating which diffracts the dressing light. The diffraction transfers recoil momentum and energy to the atoms, which results in a growth of the grating and therefore the number of atoms in the recoil mode—this is the intuitive picture for atom gain. If no atoms are injected, the whole process may start from spontaneous scattering as superradiance. We will discuss in Sec. VIII that the build-up of the matter wave grating can be induced also by a probe light beam resulting in optical amplification.

Eq. 7 describes the scattering rate out of a condensate into a recoil state with population N_q . In the limit of an empty mode for the scattered light ($n_{k-q} = 0$), it reduces to

$$W_+ = \frac{2\pi}{\hbar} |C|^2 N_0 n_k (N_q + 1) \delta(E_k - E_{k-q} - \hbar\omega_q^B). \quad (44)$$

For the high momentum transfers considered here (on the order of the photon recoil momentum), $S(q) = 1$. Each scattering event which transfers momentum $\hbar\mathbf{q}$ to the condensate, generates a recoiling atom in mode q . The final states of the photon which are associated with a momentum transfer $\hbar\mathbf{q}$ form a continuum. Integrating W_+ over all such final states gives the growth rate \dot{N}_q for the recoiling atoms. Using Eq. 41 we obtain

$$\dot{N}_q = G_q (N_q + 1) - \Gamma_{2,q} N_q \quad (45)$$

with the gain coefficient

$$G_q = R N_0 \frac{\sin^2 \theta_q}{8\pi/3} \Omega_q. \quad (46)$$

The solid angle Ω_q reflects the number of photon modes which are excited together with a quasiparticle with momentum $\hbar\mathbf{q}$. N_0 is the number of atoms in the condensate at rest and θ_q is the angle between the polarization of the dressing beam and the direction of photon emission. In addition, a loss term $\Gamma_{2,q}$ was included which describes the decoherence rate of the matter-wave grating and determines the threshold for exponential growth. It represents the linewidth of the two-photon process which generates recoil atoms in mode q . The total scattering rate W_{tot} is

$$W_{\text{tot}} = \sum_q \dot{N}_q \quad (47)$$

It is important to realize how the solid angle is divided into a sum over modes q . When $N_q \ll 1$, the sum in Eq. 47 is simply an integral over the whole solid angle and the result (without the loss term) is the Rayleigh scattering rate: $W_{\text{tot}} = \Sigma \dot{N}_j = RN_0$. However, when the build-up of population N_q becomes important, the division of the solid angle into “coherent pieces” becomes essential. The light, emitted into the direction $\mathbf{k}-\mathbf{q}$, and the quasi-particles are created in the finite volume of the condensate. Therefore, their momentum is only defined to within \hbar over the dimension of the condensate. Each “mode” represents a solid angle corresponding to that uncertainty (the longitudinal momentum of the photon is determined by energy conservation, i.e., the δ function in Eq. 44). Therefore, each scattering mode spans a diffraction limited solid angle which is approximately $\Omega_q \approx \lambda^2/A_q$ where λ is the wavelength of the scattered light and A_q is the cross-section of the condensate perpendicular to the axis of light emission.

Our Les Houches notes discuss a semiclassical derivation of the gain mechanism [10]. In this picture, one has N_q atoms in the recoil mode interfering with the condensate at rest resulting in a modulated density. When this atomic distribution is illuminated with the dressing light, all the atoms can be regarded as driven oscillators. Their radiation interferes constructively in the direction θ_q in which the density grating diffracts the dressing light. The phase-matching condition is fulfilled for this direction and a solid angle Ω_q around it. This angle can be rigorously obtained from the usual phase-matching integral for superradiance in extended samples [46]

$$\Omega_q = \int d\Omega(\mathbf{k}) \left| \int \tilde{\rho}(\mathbf{r}) \exp(i(\mathbf{k}_i - \mathbf{k}) \cdot \mathbf{r}) d\mathbf{r} \right|^2, \quad (48)$$

where \mathbf{k}_i is the wave vector of the incident light, $|\mathbf{k}| = |\mathbf{k}_i|$, and $\tilde{\rho}(\mathbf{r})$ is the normalized atomic density distribution ($\int \tilde{\rho}(\mathbf{r}) d\mathbf{r} = 1$).

The key results of the discussion above are the gain equations, Eqs. 45 and 46. For a condensate of cross-section A_q and length l_q , the gain is proportional to $N_0\Omega_q \approx \rho_0\lambda^2l_q$ which is proportional to the resonant optical density of the condensate along the direction of the scattered light. Therefore, for an anisotropic condensate, the gain is largest when the light is emitted along its longest axis (the “end-fire mode” [47]). When the intensity of the dressing light is above threshold ($G_q > \Gamma_{2,q}$ in Eq. 45), a condensate will emit highly directional beams of light and atoms along the direction for which the gain is highest. Our observation of this phenomenon has been described in Refs. [10,14].

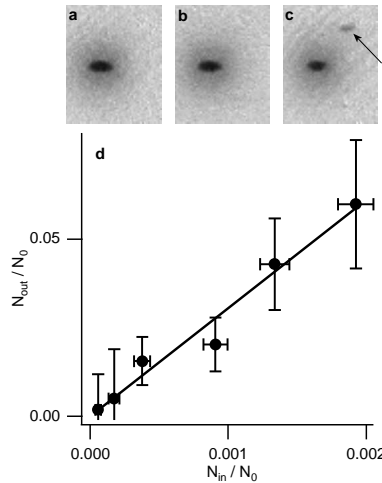


FIG. 15. Input–output characteristic of the matter-wave amplifier. (a–c) Typical time-of-flight absorption images demonstrating matter wave amplification. The output of the seeded amplifier (c) is clearly visible, whereas no recoiling atoms are discernible in the case without amplification (a) or amplification without the input (b). The size of the images is 2.8 mm \times 2.3 mm. (d) Output of the amplifier as a function of the number of atoms at the input. A straight line fit shows a number gain of 30. Reprinted by permission from Nature, Ref. [17], copyright 1999 Macmillan Magazines Ltd.

The amplification of atoms is conceptionally even simpler: Atoms in a certain recoil mode q are injected into the condensate and are amplified with a gain coefficient G_q . We only summarize the main experimental results—for a full account see Refs. [10,17].

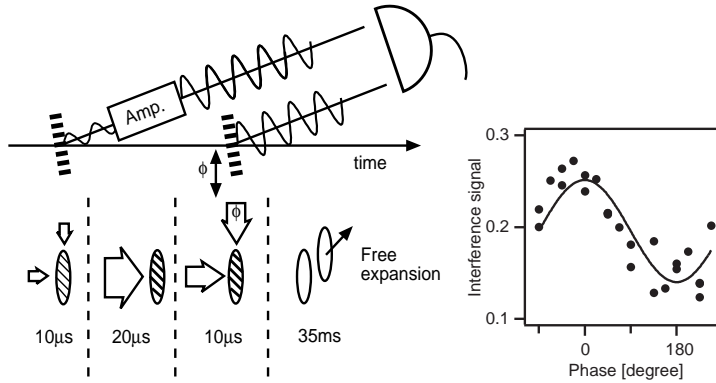


FIG. 16. Experimental scheme for observing phase coherent matter wave amplification. A small-amplitude matter wave was split off the condensate by applying a pulse of two off-resonant laser beams (Bragg pulse). This input matter wave was amplified by passing it through the condensate pumped by a laser beam. The coherence of the amplified wave was verified by observing its interference with a reference matter wave, which was produced by applying a second (reference) Bragg pulse to the condensate. The total number of atoms in the recoil mode showed constructive and destructive interference between the amplified input and the reference matter wave as the phase of the reference wave was scanned. Reprinted by permission from Nature, Ref. [17], copyright 1999 Macmillan Magazines Ltd.

Input matter waves with momentum $\hbar\mathbf{q}$ were produced by exposing the condensate to two laser beams. Their difference frequency was tuned to the resonance for Bragg scattering (see Sec. II). The stimulated redistribution of photons among the two beams transferred recoil momentum to the atoms. The fraction of atoms in the recoil state was controlled by the intensity and duration of the Bragg pulse. While these input atoms were still in the condensate volume, they were amplified when the condensate was exposed to the dressing beam. Fig. 15 shows the input-output characteristics of the amplifier. The gain was controlled by the intensity of the pump pulse (see Eq. 46) and typically varied between 10 and 100. Fig. 15d shows the observed linear relationship between the atom numbers in the input and the amplified output with a number gain of 30.

This atom amplifier is a narrow band amplifier. It only amplifies input momentum states which can be populated by condensate atoms by scattering a photon of the dressing beam. The possible input states lie on a sphere in momentum space. Its center is displaced from the origin (the momentum of the condensate at rest) by the momentum $\hbar\mathbf{k}$ of the dressing beam. The thickness of the momentum sphere is determined by the momentum uncertainty of the condensate, which is \hbar over its size, as was directly measured using Bragg spectroscopy [20]. In our experiment, the input momentum was automatically matched to the amplifier's narrow bandwidth since the input beam was created by Bragg scattering, and one of the Bragg beams was identical to the dressing beam.

The Hamiltonian in Eq. 1 provides *coherent* coupling between the light and atoms. Therefore, the atom amplification should be phase-coherent. This was experimentally verified with an interferometric technique. For this, a reference matter wave was split off the condensate in the same way as the first (input) wave (see Fig. 16). The phase of the reference matter wave was scanned by shifting the phase of the radio-frequency signal that drove the acousto-optic modulator generating the axial Bragg beam. We then observed the interference between the reference and the amplified matter waves by measuring the number of atoms in the recoil mode.

VIII. AMPLIFICATION OF LIGHT IN A DRESSED CONDENSATE

A dressed condensate (Fig. 17), a condensate illuminated by laser light, was used as an atom amplifier. Now we develop this picture further. Rayleigh scattering produces scattered photons and recoiling atoms. In the dressed atom picture, this is described as the decay of the dressed condensate into a photon and recoiling atom, or in other words, the dressed condensate can spontaneously emit pairs of photons and atoms. The amplification of atoms discussed in the previous sections solely focuses on the recoiling atoms “emitted” by the dressed condensate. Although recoiling atoms and scattered photons are emitted in pairs, the photons leave the condensate almost instantaneously and there is no significant population build-up. Formally, as discussed in the Les Houches notes, one can adiabatically eliminate the light field from coupled equations and obtain the gain equation for the matter waves.

On the other hand, the dressed condensate should act also as an amplifier for light. An input optical field should stimulate Rayleigh scattering processes which results in photons scattered into the input mode. Our recent experiments

on optical amplification in a BEC [18] required a more general description of the interplay between optical and matter wave amplification.

On the following pages, we present a general discussion of four-wave mixing of light and atoms. We first start simply with the gain cross-section for the light and a complex index of refraction. The recoiling atoms enter the picture in two stages, first within the framework of Heisenberg equations in the undepleted-pump approximation, and then using optical Bloch equations.

A. Cross-section for optical gain and slow light

The physical picture behind the optical gain of the dressed condensate is as follows: if a very weak probe beam is injected into the dressed condensate, it acts together with the dressing beam as a pair of Bragg beams and creates recoiling atoms. This process transfers photons from the dressing beam into the probe beam. At higher gain, the recoiling atoms become significant. They move out of the condensate (or decohere) on a time scale Γ_2^{-1} which is the inverse of the linewidth of the Bragg transition. In steady state, the number of recoiling atoms N_q in the volume of the condensate is proportional to the intensity of the probe light. Those recoiling atoms interfere with the condensate at rest and form a diffraction grating which diffracts the dressing beam into the path of the probe light resulting in amplification of the probe light (Fig. 17).

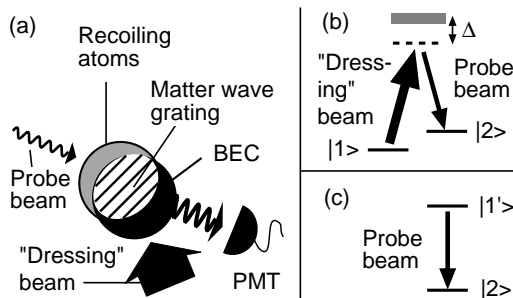


FIG. 17. Amplification of light and atoms by off-resonant light scattering. (a) The fundamental process is the absorption of a photon from the “dressing” beam by an atom in the condensate (state $|1\rangle$), which is transferred to a recoil state (state $|2\rangle$) by emitting a photon into the probe field. The intensity in the probe light field was monitored by a photomultiplier. (b) The two-photon Raman-type transition between two motional states ($|1\rangle, |2\rangle$) gives rise to a narrow resonance. (c) The dressed condensate is the upper state ($|1'\rangle$) of a two-level system, and decays to the lower state (recoil state of atoms, $|2\rangle$) by emitting a photon. Figure is taken from Ref. [18]

An expression for the gain can be derived in analogy to a fully inverted two-level system with dipole coupling which would have a gain cross-section of $6\pi\lambda^2$ for radiation with wavelength $\lambda(= 2\pi\lambda)$. For the Raman-type system in Fig. 17b, the gain is reduced by the excited state fraction, R/Γ (where R is the Rayleigh scattering rate for the dressing beam and Γ is the linewidth of the single-photon atomic resonance) and increased by Γ/Γ_2 , the ratio of the linewidths of the single-photon and two-photon Bragg resonances. Thus the expected cross-section for gain is

$$\sigma_{\text{gain}} = 6\pi\lambda^2 \frac{R}{\Gamma_2}. \quad (49)$$

The lineshape of the optical gain is that of the two-photon Bragg resonance. Due to the long coherence time of a condensate, it has a very narrow linewidth. Such a narrow band gain is accompanied by a slow group velocity of light. This can be described by a complex index of refraction $n(\omega) = n_1(\omega) + in_2(\omega)$.

For a Lorentzian resonance curve with FWHM of Γ_2 for the gain, the complex index of refraction is

$$n(\omega) = n_\infty + \frac{g'}{\delta + i} = n_\infty + \frac{g'\delta}{1 + \delta^2} - \frac{g'i}{1 + \delta^2} \quad (50)$$

where n_∞ is the background index of refraction, g' denotes the strength of the resonance, and $\delta = (\omega - \omega_0)/(\Gamma_2/2)$ is the normalized detuning from the resonance at ω_0 . The imaginary part of Eq. 50 has the usual Lorentzian lineshape.

The real and imaginary parts of the index of refraction are connected by Kramers-Kronig relations. For the special case above of a Lorentzian lineshape the gain and dispersion at resonance are connected by

$$\left. \frac{dn_1}{d\omega} \right|_{\omega=\omega_0} = -\frac{2}{\Gamma_2} n_2 \Big|_{\omega=\omega_0}. \quad (51)$$

A steep slope of the (real part of) the index of refraction gives rise to a slow group velocity of light

$$v_g = \frac{c}{\omega(dn_1/d\omega) + n_1}. \quad (52)$$

Eqs. 51 and 52 imply a simple relationship between the gain and delay time for an optical pulse. The amplitude of an optical pulse at frequency ω_0 which propagates through a medium with the index of refraction n of length l is amplified by a factor

$$g = \exp(-n_2\omega_0 l/c). \quad (53)$$

When the first term in the denominator of Eq. 52 is dominant, the delay time τ_D of the pulse is

$$\tau_D = \frac{l}{v_g} \approx l \frac{\omega_0}{c} \frac{dn_1}{d\omega} = \frac{2 \ln g}{\Gamma_2}. \quad (54)$$

This equation provides a simple relationship between a narrow band gain and pulse delay [48]. A non-inverted absorptive two-level system gives rise to “superluminal” pulse propagation [49].

For the experimental study of the optical gain, a condensate was illuminated (“dressed”) with a single off-resonant laser beam and probed with another laser beam, which was red-detuned by 91 kHz to satisfy the Bragg resonance condition. Both the dressing beam and the probe beam were in the plane perpendicular to the long axis of the condensate, and intersected at an angle of 135 degrees. The probe beam, which propagated parallel to the axis of imaging, was much larger than the condensate size. In order to block all the light that did not pass through the condensate, a slit was placed at an intermediate imaging plane. The light transmitted by the slit was recorded with a photomultiplier. The polarization of each beam was set parallel to the long axis of the condensate to suppress superradiance to other recoil modes [14].

Fig. 18 shows that light pulses were delayed by about 20 μs across the 20 μm wide condensate corresponding to a group velocity of 1 m/s. This is one order of magnitude slower than any value reported previously (see Ref. [50] and references therein). Fig. 18b presents the experimental verification of the relationship between gain and delay time (Eq. 54).

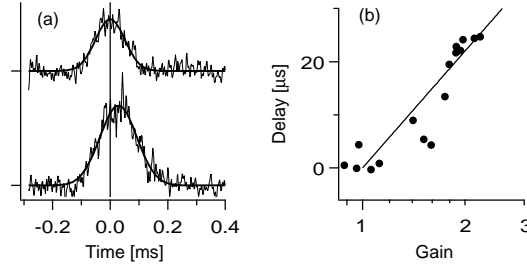


FIG. 18. Pulse delay due to light amplification. (a) About 20 μs delay was observed when a Gaussian pulse of about 140 μs width and 0.11 mW/cm^2 peak intensity was sent through the dressed condensate (bottom trace). The top trace is a reference taken without the dressed condensate. Solid curves are Gaussian fits to guide the eyes. (b) The observed delay was proportional to the logarithm of the observed gain. Figure is taken from Ref. [18].

B. Relation between optical gain and atomic gain

Both the optical gain g (Eqs. 49 and 53) and the matter wave G gain (Eq. 46) have the same origin, stimulated Rayleigh scattering. Therefore, the two gain coefficients should be related. The expression for G (Eq. 46) involves a solid angle factor Ω_q which is proportional to λ^2/A . To be consistent with the optical Bloch equation (to be discussed below) we use now $2\lambda^2/A$ for Ω_q and obtain

$$G = \frac{RN_0}{A} \frac{3}{4\pi} \lambda^2 = (\rho_0 l \sigma_{\text{gain}}/2) \Gamma_2. \quad (55)$$

The gain g for the amplitude of the optical field is

$$g = \exp(\rho_0 l \sigma_{\text{gain}}/2) = \exp(G/\Gamma_2) \approx 1 + \frac{G}{\Gamma_2} \quad (56)$$

with the last equation being an approximation for small gain. However, Eq. 56 cannot be universally valid. When the gain G is above the threshold for superradiance, $G > \Gamma_2$ (Eq. 45) the optical gain should diverge: a single recoiling atom created by the probe light and dressing light is exponentially amplified and creates a huge matter wave grating which will diffract the dressing light into the probe light path, thus amplifying the probe light by a divergent factor. Indeed, as we will derive below, Eq. 56 is only valid at small values of G/Γ_2 .

If we can neglect the depletion of the dressed condensate and the dressing laser beam we can simplify the interaction Hamiltonian in Eq. 1 to

$$\mathcal{H}' = C'(\hat{a}^\dagger \hat{c}^\dagger + \hat{a} \hat{c}). \quad (57)$$

Here, $\hat{a}(\hat{c})$ indicates the atomic (light) field to be amplified, but the following derivation is completely symmetric between the two fields. This Hamiltonian is a standard down-conversion Hamiltonian. Here it describes the down-conversion of the dressed condensate into photons and recoiling atoms. Considering only two modes neglects propagation effects in the amplification. The coefficient C' defines the time constant of the amplification and is proportional to the amplitude of the dressing beam and the square root of the number of atoms in the condensate. The Heisenberg equations of motions are

$$i\dot{\hat{a}} = [\hat{a}, \mathcal{H}'] = C' \hat{c}^\dagger, \quad (58)$$

$$i\dot{\hat{c}}^\dagger = [\hat{c}^\dagger, \mathcal{H}'] = -C' \hat{a}. \quad (59)$$

This leads to exponential growth of \hat{a} and \hat{c} (proportional to $\exp(C't)$). However, to describe the physical situation in the experiments, one has to allow for damping by introducing $\Gamma_a(\Gamma_c)$ as phenomenological damping time constants for $\hat{a}(\hat{c})$. We also include source terms (input fields) and approximate the operators by c numbers:

$$\begin{aligned} \dot{a} &= -\frac{\Gamma_a}{2}(a - a_0) - iC'c^*, \\ \dot{c}^* &= iC'a - \frac{\Gamma_c}{2}(c^* - c_0^*). \end{aligned} \quad (60)$$

The solutions show relaxation ($C'^2 \leq \Gamma_a \Gamma_c/4$) or exponential growth ($C'^2 \geq \Gamma_a \Gamma_c/4$) depending on the strength of the coupling relative to the damping rates. The “gain” below the threshold can be defined as $a(t \rightarrow \infty)/a_0$ for atoms (assuming $c_0 = 0$) and as $c(t \rightarrow \infty)/c_0$ for light (assuming $a_0 = 0$), yielding

$$g = \frac{a(t \rightarrow \infty)}{a_0} = \frac{c(t \rightarrow \infty)}{c_0} = \frac{\Gamma_a \Gamma_c/4}{(\Gamma_a \Gamma_c/4) - C'^2}. \quad (61)$$

The fact that the two gain coefficients are equal is a general property of parametric amplification where two kinds of particles are produced in pairs.

In the limiting case that one field is strongly damped (e.g. that light quickly escapes from the system, $\Gamma_c \gg \Gamma_a$), one can adiabatically eliminate this field from the coupled equation (assuming no photon input ($c_0^* = 0$))

$$c^* = \frac{2iC'}{\Gamma_c} a \quad (62)$$

and obtain a single gain equation for a . The gain equation for the atom field is

$$\dot{a} = -\frac{\Gamma_a}{2}(a - a_0) + \frac{2C'^2}{\Gamma_c} a. \quad (63)$$

In the absence of damping, the atom number would increase exponentially with a rate constant $4C'^2/\Gamma_c$ which we therefore identify with the atom gain rate coefficient G in Eq. 55. This can be shown explicitly using $C'^2 = |C|^2 N_0 n_k / \hbar^2$ and setting the mode volume $V = AL$, where A is the cross section of the condensate. The axial length L could be the condensate length l , but will cancel out. Eqs. 34 and 43 yield $4C'^2/\Gamma_c = 2Gc/L\Gamma_c$ which equals G when we set the decay rate $\Gamma_c/2$ equal to the photon transit time c/L . We can then rewrite the gain calculated above as

$$g = \frac{\Gamma_a}{\Gamma_a - 4C'^2/\Gamma_c} = \frac{\Gamma_a}{\Gamma_a - G}. \quad (64)$$

For the dressed condensate, we identify Γ_a with Γ_2 . As expected, at the threshold to superradiance ($G = \Gamma_2$), the (steady-state) gain for both light and matter waves diverges. The gain can be rewritten as

$$g = \Gamma_2/(\Gamma_2 - G) = 1 + G/(\Gamma_2 - G). \quad (65)$$

In the low gain limit, this yields the same result as Eq. 56. The comparison with Eq. 56 shows that the effect of the coupled equations is to replace the two-photon linewidth Γ_2 in Eq. 56 by the dynamic coherence decay rate $\Gamma_2 - G$. Since propagation effects have been excluded, we can't expect to obtain the exponential factor in Eq. 56, but rather the linearized form. The expansion

$$g = 1 + (G/\Gamma_2) + (G/\Gamma_2)^2 + \dots \quad (66)$$

describes the transition from (linear) single-atom gain to (nonlinear) collective gain.

C. Optical Bloch equations

The discussion in the previous two sections assumed that the condensate is undepleted—i.e., we calculated properties of a condensate with all the atoms in the initial dressed state. However, the presence of the dressing light and the probe light depletes the condensate. Furthermore, the calculated amplification coefficients are only valid in a quasi-steady state regime which is usually preceded by transient behavior. A correct interpretation of the experimental results required a more complete description of the dynamics of the system which will be developed in this section using optical Bloch equations.

We proceed in two steps. In the limit of weak optical gain (or strong probe laser intensity), we will use the ordinary optical Bloch equations where the laser fields are treated as constant. Later we will introduce an additional equation for the dynamics of the probe light. The condensate at rest ($|1\rangle$) and the atoms in the recoil state ($|2\rangle$) are treated as a two-level system coupled by the four-wave mixing Hamiltonian which gives rise to a two-photon Rabi frequency Ω_R (Eq. 33). The coherence between those two states decays at a rate $\Gamma_2/2$. Assuming constant Ω_R , the optical Bloch equations at resonance take the following simple form

$$\dot{v} = -\frac{\Gamma_2}{2}v - \Omega_R w \quad (67)$$

$$\dot{w} = \Omega_R v \quad (68)$$

where $v = 2 \operatorname{Im}(\rho_{12})$ represents the amplitude of the matter wave grating (ρ_{ij} is the atomic density matrix) and $w = \rho_{22} - \rho_{11}$ is the population difference between the two states [51].

The eigenvalues of the matrix

$$\begin{pmatrix} -\Gamma_2/2 & -\Omega_R \\ \Omega_R & 0 \end{pmatrix} \quad (69)$$

are $\lambda_{\pm} = -\Gamma_2/4 \pm \sqrt{(\Gamma_2/4)^2 - \Omega_R^2}$. In the limits of large and small laser intensities one obtains

$$\lambda_{\pm} = \begin{cases} -\frac{\Gamma_2}{4} \pm i\Omega_R & \Gamma_2/4 \ll \Omega_R \\ -\frac{\Gamma_2}{2}, -\frac{2\Omega_R^2}{\Gamma_2} & \Gamma_2/4 \gg \Omega_R \end{cases}. \quad (70)$$

This means that at high intensities the system exhibits damped oscillations—Rabi oscillations between the two levels. At low intensities, there is relaxation in two steps: The coherence is damped with a rate of $\Gamma_2/2$, followed by depletion of atoms in the condensate, which happens at a rate of $2\Omega_R^2/\Gamma_2$. It is in this temporal window ($2/\Gamma_2 < t < \Gamma_2/2\Omega_R^2$) that the perturbative treatment with the complex index of refraction applies. For longer times, the condensate becomes depleted and the assumption that most of the atoms are in the initial dressed state is no longer valid.

The optical Bloch equations can be analytically solved for a step function input. With the initial condition that at time $t = 0$ all the atoms are in the condensate at rest ($w(t = 0) = -1$, $v(t = 0) = 0$) one obtains

$$v(t) = \begin{cases} \frac{\Omega_R}{\sqrt{\Omega_R^2 - (\Gamma_2/4)^2}} \exp(-\frac{\Gamma_2}{4}t) \sin\left(\sqrt{\Omega_R^2 - (\Gamma_2/4)^2}t\right) & \Omega_R \geq \frac{\Gamma_2}{4} \\ \frac{\Omega_R}{\sqrt{(\Gamma_2/4)^2 - \Omega_R^2}} \exp(-\frac{\Gamma_2}{4}t) \sinh\left(\sqrt{(\Gamma_2/4)^2 - \Omega_R^2}t\right) & \Omega_R \leq \frac{\Gamma_2}{4} \end{cases} \quad (71)$$

simplifying in the limit of small probe laser intensity ($\Omega_R \ll \Gamma_2/4$) to

$$v(t) \approx \frac{2\Omega_R}{\Gamma_2} \left(-\exp(-\frac{\Gamma_2}{2}t) + \exp(-\frac{2\Omega_R^2}{\Gamma_2}t) \right) \quad (72)$$

$$= \frac{2\Omega_R}{\Gamma_2} \left(-\exp(-\frac{\Gamma_2}{2}t) + 1 \right) \quad t \ll \Gamma_2/\Omega_R^2. \quad (73)$$

By reducing the probe power, the Rabi oscillations slow down and become overdamped and a (quasi-)steady state gain is obtained. Inserting Eq. 72 into Eq. 68 one obtains the transition rate $N_0\dot{w}/2 = N_0\Omega_R v/2$ which is the number of photons per unit time emitted by the dressed condensate. To obtain the gain one has to normalize by the input photon flux cn_p/l where n_p is the number of photons in the condensate. The amplitude gain is then (assuming small gain)

$$g = 1 + \frac{N_0\Omega_R l}{4cn_p} v. \quad (74)$$

Using the asymptotic behavior of Eq. 73 ($v(t) \approx 2\Omega_R/\Gamma_2$), Eq. 43 for Ω_R and Eq. 49 one obtains $g = 1 + \rho_0\sigma_{\text{gain}}l/2$ which agrees with Eqs. 56 and 65 in the low-intensity limit. Eq. 74 thus has the correct asymptotic limit, but it also describes transient behavior when the general solution for $v(t)$ (Eq. 71) is used. Theoretical traces based on Eq. 74 are directly compared to the experimental results in Fig. 19.

In the experiment, we used long square probe pulses for the probe light (Fig. 19). When the dressing beam was suddenly switched off, a sudden change in the observed probe light intensity was evidence for optical gain. At the lowest probe intensity, the depletion of atoms in the condensate was negligible and a clear step at the switch off was observed, corresponding to a gain of ≈ 2.8 . The initial rise time of $\approx 100 \mu\text{s}$ is the coherence time of the dressed condensate. At high probe laser power we observed Rabi oscillations in the transmitted probe light. Note that all the traces were normalized by the probe beam intensity, and the oscillatory trace at the bottom was obtained at the highest probe beam intensity. The oscillations reflect simple two-level Rabi oscillations of atoms between the two motional states driven by the two-photon Bragg coupling.

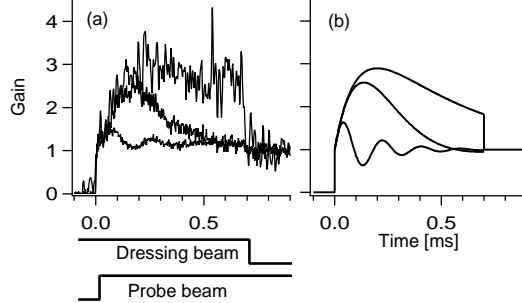


FIG. 19. Gain and temporal behavior of light pulses propagating through a dressed condensate. (a) Observed probe pulse output from a dressed condensate. The probe light intensities were 5.7 mW/cm^2 (bottom), 1.5 mW/cm^2 (middle), 0.10 mW/cm^2 (top), while the dressing beam intensity was 5 mW/cm^2 , which was just below the threshold for superradiance. The plotted signals were normalized by the incident probe intensity and show the gain for the probe light. (b) Calculated probe light output for typical experimental parameters. Rabi oscillations develop into steady state gain as the intensity of the probe light is reduced. Figure is taken from Ref. [18].

When the probe laser frequency was detuned from the two-photon resonance, the frequency of the Rabi oscillations increased (Fig. 20). Optical Bloch equations with detuning [51] predict oscillations at

$$\Omega_{\text{eff}} = \sqrt{\Omega_R^2 + \Delta\omega^2} \quad (75)$$

where $\Delta\omega$ is the detuning, in agreement with observations.

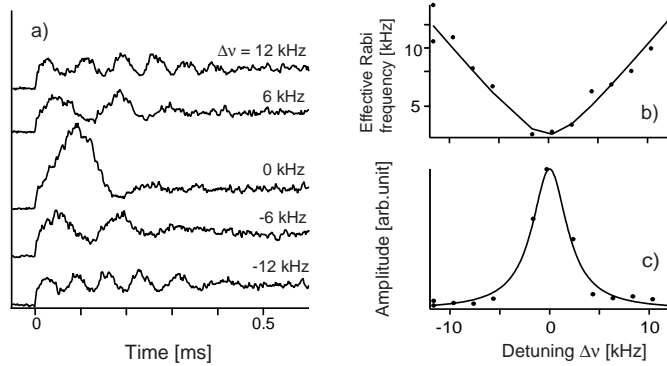


FIG. 20. Rabi oscillations of atoms observed by monitoring the transmitted probe light intensity. a) Rabi oscillations for different detunings of the probe light from the two-photon resonance. b) Observed frequencies of Rabi oscillation versus detuning. The solid line is a fit to Eq. 75. c) Amplitude of the oscillations versus detuning. The solid line is a Lorentzian fit with a linewidth of about 4 kHz.

For large optical gain, the Rabi frequency Ω_R increases during the pulse and the above treatment is no longer valid. Therefore, we derive now a second equation which treats the Rabi frequency as a dynamic variable. The population transfer to the recoil state (\dot{w}) results in an increase of the number of the probe beam photons inside the condensate volume

$$\dot{n}_p = c(n_p^0 - n_p)/l + N_0\dot{w}/2, \quad (76)$$

where l is the length of the condensate with N_0 atoms and cn_p^0/l is the input photon flux. Without gain, the steady-state number of photons in the condensate volume would be n_p^0 . Eq. 76 neglects propagation effects of the light by replacing the non-uniform electric field by an average value (such a “mean-field model” is only qualitative, see [52]).

Replacing the photon number by the Rabi frequency (Eq. 43) leads to

$$2\Omega_R\dot{\Omega}_R = \frac{c}{l}(\Omega_0^2 - \Omega_R^2) + \frac{N_0}{2} \frac{R6\pi\lambda^2 c}{V} \Omega_R v \quad (77)$$

where Ω_0 is the two-photon Rabi frequency due to the input probe beam and the dressing beam. For small gain, we approximate $\Omega_0^2 - \Omega_R^2 \approx 2\Omega_R(\Omega_0 - \Omega_R)$. This approximation should retain the qualitative features of the coupled light-atom system even when the small gain approximation is no longer quantitative. Indeed, we will obtain results consistent with our previous treatment (Eq. 65) which was not limited to small gain. Using Eq. 55 for the atom gain G we obtain

$$\dot{\Omega}_R = \frac{c}{l}(\Omega_0 - \Omega_R + \frac{G}{2}v) \quad (78)$$

This equation together with Eqs. 67 and 68 forms a set of coupled equations describing the combined dynamics of the atom and light fields. The situation is analogous to the optical laser, where the atomic polarization and the electric field inside the cavity are coupled. However, the role of atoms and light is reversed: in the optical laser, the cavity lifetime is usually longer than the coherence time of the atomic polarization, whereas in our case the extremely long coherence time of the condensate dominates. This would correspond to the bad cavity limit of the optical laser which is usually not realized (see [53] and references therein).

Assuming rapid relaxation of the light field ($\dot{\Omega}_R = 0$ in Eq. 78) leads to

$$\Omega_R = \Omega_0 + \frac{G}{2}v. \quad (79)$$

Inserting this into Eqs. 67 and 68 adiabatically eliminates the light field. This treatment is more general than the Heisenberg equations above, where we had neglected condensate depletion. To check for consistency, we now assume an undepleted condensate ($w = -1$) and obtain

$$\dot{v} = \frac{G - \Gamma_2}{2}v + \Omega_0. \quad (80)$$

Below the threshold for superradiance, ($G \leq \Gamma_2$), v relaxes with a time constant of $2/(\Gamma_2 - G)$ to $v = 2\Omega_0/(\Gamma_2 - G)$. This and Eq. 79 show that the gain g for the probe beam is

$$g = 1 + \frac{G}{\Gamma_2 - G} \quad (81)$$

in agreement with Eq. 65.

D. Optical probe of matter wave gain

The matter wave grating formed inside the condensate is responsible for both atomic and optical gain. We now briefly describe experiments where the dynamics of the matter wave grating could be directly observed by monitoring the probe light. We first created a matter wave grating with a Bragg pulse and then observed its time evolution by monitoring the diffracted dressing beam. The initial seed pulse was $100 \mu\text{s}$ long and transferred about 5% of the atoms to the recoil state.

At lower intensities for which atom amplification was negligible, the grating showed a simple decay (Fig. 21). At higher intensities, collective gain started to compensate the loss, and at intensities above a threshold, net amplification was observed. The initial growth rate (Fig. 21) followed the linear dependence on the intensity of the dressing beam ($\propto (G - \Gamma_2)$) predicted by Eq. 80 and Refs. [14,54]. The net growth of the matter wave grating was studied previously by observing an increase in the number of recoiling atoms in time-of-flight images [17], whereas Fig. 21 was obtained by monitoring the dynamics of amplification *in situ* by observing light instead of atoms.

Extrapolating the decay rate in Fig. 21 to zero intensity of the dressing beam gives the decay rate of the matter wave grating Γ_2 of $(100 \mu\text{s})^{-1}$, in fair agreement with the linewidth of the Bragg excitation process observed previously [20]. This observation of the decay of the matter-wave grating can be regarded as pump-probe spectroscopy of quasi-particles in the condensate. The seeding Bragg pulse created the quasi-particles (in this case condensate excitations in the free-particle regime). One can control the momentum of the excited quasi-particles by the angle between the laser beams. This could be used to excite phonon-like quasiparticles [15], and their lifetimes could be determined with the pump-probe scheme presented here.

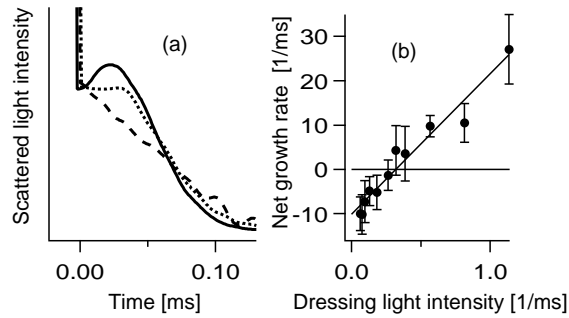


FIG. 21. Pump-probe spectroscopy of a matter wave grating inside the condensate. (a) First, approximately 5 % of atoms were transferred to the recoil state by the two-photon Bragg transition. Then the dynamics of the matter wave grating was observed *in situ* by illuminating the grating with off-resonant dressing light and monitoring the diffracted light intensity. All traces were normalized to the same diffracted light intensity at $t = 0$. The dressing beam intensity was 2.9 mW/cm^2 (bottom), 5.7 mW/cm^2 (middle), 13 mW/cm^2 (top). (b) The initial growth rate of the grating vs. light intensity shows the threshold for net gain. The intensity of the dressing beam is given in units of the single-atom Rayleigh scattering rate. Figure is taken from Ref. [18].

E. Single-atom and collective behavior

The optical gain studied above clearly showed the transition from single-atom gain (the first term in the expansion in Eq. 66) to collective gain. Varying the intensities of probe and dressing light allows for the study of different physical regimes. At low dressing light intensity, below the superradiant threshold, one encounters single-atom behavior, at high intensity the system shows collective superradiance. The probe laser intensity determines whether the system

shows oscillatory or steady state response, as derived above using optical Bloch equations. Fig. 22 summarizes the different regimes.

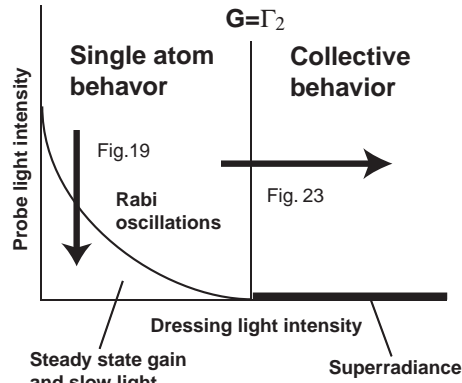


FIG. 22. Schematic diagram of the different regimes of a dressed condensate. Depending on the intensities of the dressing and the probe beams, the dressed condensate occupies different physical regimes. Single atom and collective behavior are separated by the threshold to superradiance ($G = \Gamma_2$, Eq. 45).

Probe light traces showing the transition from Rabi oscillations to superradiance are presented in Fig. 23. As a function of the dressing light intensity, the damped Rabi oscillations become faster and almost suddenly turn into a giant superradiant pulse.

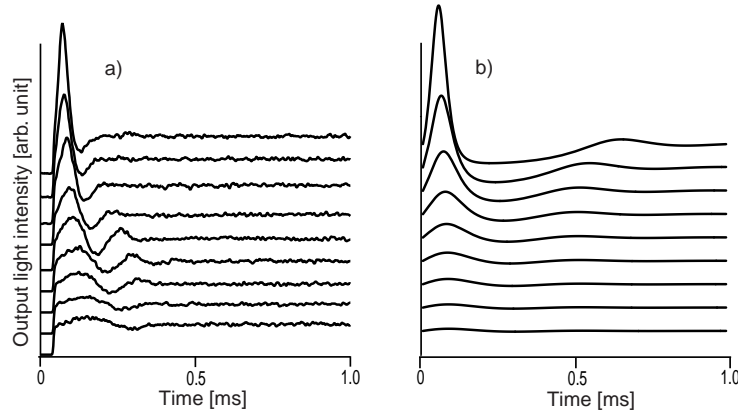


FIG. 23. From single-atom Rabi oscillations to collective superradiance. a) The dressing beam intensity was increased from 2.7, 3.8, 6.1, 9.1, 14.1, 21.3, 32.7, 49.5 to 76 mW/cm² (bottom to top). The probe beam intensity was kept at 5 mW/cm². b) Numerical solution of the nonlinear optical Bloch equations (Eqs. 78, 67 and 68). Plotted is Ω_R^2 for the same experimental parameters as in a).

Previously, recoil related gain based on single-atom phenomena (Recoil Induced Resonances) was observed in cold cesium atoms [55]. Collective gain due to the formation of a density grating was discussed as a possible gain mechanism for lasing action [56] (named CARL—Coherent Atomic Recoil Laser) and pursued experimentally [57,58] with ambiguous results (see [59] and the discussion in [60,61]). Our experiments clearly identify the two regimes and their relationship.

The dressed condensate is a clean, model system for discussing optical and atom-optical properties. The observed slow group velocity of the probe laser pulse can be directly related to the dynamics of the amplification process. The optical amplification can be described as a reflection of the dressing light by a matter wave grating. The initial delay time in the amplification of optical pulses is the time necessary to build up the (quasi-)steady state matter wave grating. When the input pulse is switched off, the matter wave grating still exists and diffracts the pump light (as observed in Fig. 21) creating the trailing edge of the transmitted light pulse. Thus, the slow speed of light is simply related to the slow build-up and decay of quasi-particles which we were able to monitor directly. In this microscopic picture, all photons propagate with the vacuum speed of light c , the slow group velocity is only a phenomenological

description of the center-of-mass propagation of the amplified pulse. This description leads to the same number of photons inside the condensate. Slow light pulses are compressed by a factor c/v_g , but the electric field strength is unchanged [62,63]. Therefore, the product of the total number of photons within the pulse and the transit time is constant.

Recent demonstrations of slow group velocities for light focused on electromagnetically induced transparency (EIT) in a three-level Λ system [50]. This system features a narrow dip in a broad absorption feature. In our system, the broad absorption line is missing. Since the propagation of resonant laser pulses is mainly determined by the narrow feature (which determines $dn_1/d\omega$), both systems show analogous behavior (see Fig. 24). Indeed, if one would add a broad-band absorber to the narrow-band amplifier, one would create the same index of refraction as in the EIT scheme.

Although both schemes involve three levels in a Λ configuration (Fig. 24), there are major differences. The amplification scheme does not have a dark state because it has off-resonant couplings to other momentum states which are indicated in Fig. 24. In the amplification scheme the strong pump pulse connects the initially populated state to the excited state in a far-off resonant way. In the EIT scheme the strong coupling laser drives the other leg of the Λ transition and is on resonance.

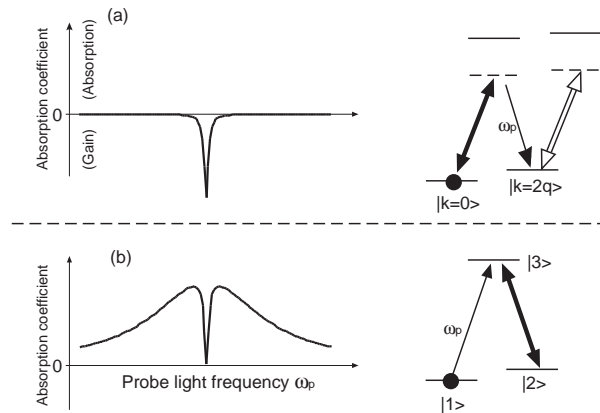


FIG. 24. Comparison between two different methods to generate slow light. (a) Narrow-band optical amplification using a two-photon resonance. (b) Electromagnetically induced transparency.

Finally, we want to resume the discussion of Sect. VI, where we presented the two limits of four-wave mixing of light and atoms which correspond to diffraction of light off an atomic grating (for $N_q > n_{k-q}$) and diffraction of atoms off an optical grating (for $N_q < n_{k-q}$). These two limits of atomic stimulation and optical stimulation reflect whether the final state occupation number is larger for atoms or photons. Therefore, we have to address what are the relevant modes and their occupation numbers. So far, we have disregarded the absolute number of photons. The coupling constant C (Eq. 36) is inversely proportional to the mode volume V , hence for the physical description it was only relevant to look at the photon density which is proportional to the electric field squared. Therefore, the system can be well described semi-classically by the coupling of an electric field (or Rabi frequency) to the atomic density, and on the previous pages, we have presented several formalisms for that.

The question of the photon number becomes relevant when we want to use the concepts of Sect. I where we have developed a formalism to describe amplification in a BEC. We showed that the scattering rate W for a condensate illuminated by a laser beam is proportional to

$$W \propto N_0 n_k (N_q + n_{k-q} + 1). \quad (82)$$

This description focuses on two modes for the photons. However, since the experiment takes place in open space with freely propagating laser beams, one has to carefully identify the relevant modes for such a description. Here we show that all the different cases of light scattering discussed in these notes, Bragg scattering, Rayleigh scattering, and the amplification of light and atoms, can be intuitively described by Eq. 82.

For Bragg scattering, the optical Bloch equations yield the steady state scattering rate as $W = N_0 \dot{w}/2 = N_0 \Omega_R v/2 = N_0 \Omega_R^2/\Gamma_2$. This is in agreement with Eq. 10 when we replace the δ function by a (normalized) Lorentzian lineshape of FWHM of Γ_2 , which has a value of $2/\pi\Gamma_2$ on resonance. Thus the rate for Bragg scattering can be written as (neglecting numerical factors and setting $S(q) = 1$ for large momentum transfer)

$$W_{\text{Bragg}} \approx (|C|/\hbar)^2 N_0 n_k (n_{k-q} + 1)/\Gamma_2. \quad (83)$$

For the amplification of atoms, the gain equation (Eq. 45) implies

$$W_{\text{atom_gain}} \approx (|C|^2/\hbar)N_0n_k(N_q + 1)\frac{d\rho}{dEd\Omega}\Omega_q. \quad (84)$$

For the amplification of light, the scattering rate at low intensity of the dressing beam is given by Eq. 83—thus we are in the regime of scattering atoms off an optical grating. The number of photons n_{k-q} in the input mode is the number of photons in a volume V with the cross section A of the condensate and a length $l_{\text{mode}} \approx c/\Gamma_2$. This choice of length is the coherence length of light with a spectral bandwidth Γ_2 . This value for l_{mode} can be justified by another argument. The coupled equations (Eq. 60) reduce the physical description to one mode of the scattered light. The angular mode selection occurs by the cigar shape of the condensate. The Bragg scattering process with a linewidth Γ_2 couples to only one longitudinal mode if we assume boundary conditions which impose a mode spacing of Γ_2 , e.g. assuming non-reflecting walls at a distance $\approx c/\Gamma_2$. To be consistent, the number of photons in the input laser beam has to be determined over the same length.

Now we want to turn to the transition from light amplification stimulated by light to light amplification stimulated by atoms. Using Eq. 43 one obtains (again neglecting numerical factors)

$$n_{k-q} \approx \Omega_R^2 A l_{\text{mode}} / R \lambda^2 c. \quad (85)$$

Expressing the Rayleigh rate R by the atom gain G (Eq. 55), $R \approx GA/N_0\lambda^2$, we get

$$n_{k-q} \approx N_0\Omega_R^2 l_{\text{mode}} / Gc \approx N_0\Omega_R^2 / G\Gamma_2. \quad (86)$$

The number N_q of recoiling atoms is approximately the Bragg scattering rate, Ω_R^2/Γ_2 times the coherence time $1/\Gamma_2$ times the number of condensate atoms N_0

$$N_q \approx N_0\Omega_R^2 / \Gamma_2^2. \quad (87)$$

Comparing Eqs. 86 and 87 we see that around the threshold for superradiance ($G = \Gamma_2$), the regime $N_q \ll n_{k-q}$ crosses over to $N_q \approx n_{k-q}$. In other words, the bosonic stimulation factor during the optical amplification, $(N_q + n_{k-q} + 1)$ (Eq. 82), is approximately n_{k-q} in the linear (single-atom) regime. Near the threshold to superradiance, the N_q term becomes significant and diverges at threshold. This statement can be generalized to include superradiance. Whenever the number of recoiling atoms N_q dominates in Eq. 82 one enters the regime of nonlinear amplification. Without a probe beam, i.e. for $n_{k-q} = 0$, nonlinear scattering and superradiance set in for $N_q \approx 1$.

The photon counting becomes even more confusing when one tries to extend it to the scattered photons. The following remarks are rather tentative and reflect hours of controversial and not fully resolved discussions. The occupation number of the adiabatically eliminated photon field in Eq. 62 is $n_{k-q} = |c^*|^2 \approx GN_q/\Gamma_c$ (with $N_q = |a|^2$). Since the gain G is the Rayleigh scattering rate into the solid angle Ω_q of the mode, we can interpret n_{k-q} as the photon number emitted into the mode during the damping time $1/\Gamma_c$ of the photon field (and stimulated by N_q atoms in the final state). The physical process is independent of the damping time Γ_c (and therefore of the absolute number n_{k-q} of photons). In our experiments, the scattered photons hit the walls of the vacuum chamber (or a photo detector) within nanoseconds.

In the case of atom amplification, all scattered photons were emitted spontaneously (in the sense of the superradiant cascade described by Dicke [74]) and should not be counted in a bosonic stimulation term. Even if these photons were emitted into a cavity, they would stimulate the emitting system only after being reflected back. However, it is precisely this photon field (Eq. 62) which leads to the bosonic stimulation by atoms (Eq. 63). The Hamiltonian (Eq. 57) couples atoms only to light. After eliminating the photon field, the (atomic) bosonic stimulation term represents the coupling of all atoms to the same mode of the electromagnetic field, and that's how the atoms stimulate each other. Rate equations (Eq. 82) only apply after coherences have damped out. The most rapidly damped mode is therefore no longer an independent degree of freedom, but slaved to the slower modes. This suggests that the photon number n_{k-q} in Eq. 82 reflects the external laser field, and not the scattered photons—they appear already in the atomic stimulation term N_q . All these conceptual problems are avoided (but not solved!) when one sticks to the coupled equations between the photon and atom fields.

If we inject probe light near the threshold to superradiance, we have optical amplification by bosonic stimulation of atoms! However, the output light intensity is still proportional to the input intensity. In steady state, the population N_q , the Rayleigh scattering rate (stimulated by these N_q atoms) and therefore the number of photons added to the probe light are all proportional to the input light intensity. The system is driven by the probe light input. It is amplified by a gain factor which includes the dynamics of the coupled atomic and optical fields.

Finally, we want to show how to obtain the Rayleigh scattering rate from Eq. 83. We assume the final photon states to be empty (setting $n_{k-q} = 0$) and multiply with the number of final states. This number $\Delta\rho$ is obtained by multiplying the density of states Eq. 38 by the linewidth $\hbar\Gamma_2$ and the full solid angle $\Delta\rho = (d\rho/dE d\Omega)(4\pi)(\hbar\Gamma_2)$. This leads to

$$W_{\text{Rayleigh}} = (|C|/\hbar)^2 N_0 n_k \Delta\rho / \Gamma_2 \approx (|C|^2/\hbar) N_0 n_k \frac{d\rho}{dE d\Omega} 4\pi, \quad (88)$$

which is approximately equal to the Rayleigh scattering rate R (Eq. 39). The stimulated Bragg scattering rate (Eq. 83) dominates over the spontaneous Rayleigh rate when the number of photons n_{k-q} in the Bragg beam is larger than the number $\Delta\rho$ of accessible modes. Note that this intuitive result is independent of defining modes and boundary conditions—the two-photon linewidth Γ_2 has cancelled out. Subtleties arise only in the case of coherent emission. In this case, one has either to describe coherent superposition states of several modes, or identify modes which reflect the linewidth of the transition.

IX. ENHANCEMENT OF SPONTANEOUS EMISSION IN A BOSE-EINSTEIN CONDENSATE

In the previous sections we have illustrated the rich physics which is described by the rate equations introduced in the first section. They suggested that the relevant matrix element is always $S(q)$, and that enhanced scattering relies on the population of the final states with several particles or photons. This and the following section broaden this picture. This section, which is a slightly modified version of a recently submitted paper [16], shows that $S(q)$ is the matrix element only for scattering particles or light, but not for spontaneous emission. Finally, Sect. X discusses that collective enhancement is not restricted to bosonic systems and macroscopic population of a quantum state.

In the previous sections we have shown that light scattering and particle scattering in a condensate can be suppressed. This suppression is due to the reduction of density fluctuations in a condensate at long wavelengths (longer than the healing length). The dissipation-fluctuation theorem implies that the same suppression can be observed in the response of a condensate to an external perturbation. Therefore, one might interpret the suppression as the “unwillingness” of a condensate against long-wavelength modulations.

A similar suppression of the long wavelength response (or reduction of the structure factor $S(q)$) occurs in degenerate Fermi gases due to Pauli blocking. Transfer of momentum comparable to or less than the Fermi momentum is suppressed due to occupancy of possible final states. Pauli blocking is a single-particle effect and would occur even in an ideal non-interacting Fermi gas. In contrast, the suppression of momentum transfer in a BEC is a genuine many-body effect due to the atomic interactions and the collective nature of the condensate. It seems that Fermi seas and condensates have similar behavior for different physical reasons.

In addition to particle and light scattering, we want to discuss now the process of spontaneous emission of an excited atom initially at rest in the condensate or the Fermi sea. For the Fermi sea, there is suppression: spontaneous emission is impossible for recoil momenta less than the Fermi momentum. Surprisingly, the situation is different for a condensate where spontaneous emission is enhanced.

This effect is most easily derived for a homogeneous condensate at zero temperature consisting of N atoms at a density ρ in a volume V . Due to the atomic interactions described by Eq. 11, two atoms in the zero-momentum state are coupled to states with momenta $+\hbar\mathbf{k}$ and $-\hbar\mathbf{k}$. The ground state wavefunction $|g\rangle$ of a BEC has admixtures of pair correlations yielding the structure [2]

$$|g\rangle = |N, 0, 0\rangle - \alpha |N-2, 1, 1\rangle + \alpha^2 |N-4, 2, 2\rangle + \dots, \quad (89)$$

where $\alpha = 1 - 1/u_k^2$. Here $|N_0, N_k, N_{-k}\rangle$ denotes a state with N_0 atoms in the zero-momentum state and $N_{\pm k}$ atoms in states with momentum $\pm\hbar\mathbf{k}$. In Eq. 89 a summation over all momenta $\hbar\mathbf{k}$ is implicitly assumed. The average population of momentum states is given by $N(k) = u_k^2 - 1 = v_k^2$, where $u_k = \cosh \phi_k$, $v_k = \sinh \phi_k$ and $\tanh 2\phi_k = \mu/(\hbar\omega_k^0 + \mu)$ as already introduced in Sect. II.

To study the effect of the presence of a BEC on spontaneous emission, we consider an excited atom at rest added to a BEC of N ground-state atoms. This system is described by an initial state $|i\rangle = \hat{a}_{e,0}^\dagger |g\rangle$, where $\hat{a}_{e,0}^\dagger$ creates an electronically excited atom at rest. We use Fermi's golden rule to obtain the rate for spontaneous emission. The only difference to the single-atom spontaneous decay rate Γ comes from the overlap matrix elements to the final momentum state $|f\rangle$, $\langle f | \hat{a}_{k_L}^\dagger \hat{a}_{e,0} | i \rangle$ where $\hat{a}_{k_L}^\dagger$ is the creation operator for a free ground state atom with momentum of the photon $\hbar\mathbf{k}_L$. Summing over all final states one arrives at

$$\gamma_{\text{BEC}} = \Gamma \langle g | \hat{a}_{k_L} \hat{a}_{k_L}^\dagger | g \rangle. \quad (90)$$

Thus, the spontaneous emission rate is proportional to the square of the norm of the state vector $|e^+\rangle = \hat{a}_{k_L}^\dagger |g\rangle$.

To calculate the norm of $|e^+\rangle$ explicitly, we transform to Bogoliubov operators (see Sect. II) and obtain

$$\begin{aligned} F_{\text{Bose}}^{\text{spont}} &= \langle e^+ | e^+ \rangle = u_{k_L}^2 = 1 + N(k_L) \\ &= \left(\cosh \left(\frac{1}{2} \tanh^{-1} \left(\frac{k_s^2}{k_L^2/2 + k_s^2} \right) \right) \right)^2, \end{aligned} \quad (91)$$

where $\hbar k_s = M c_s$ is the momentum of an atom moving at the speed of sound. Enhancement of spontaneous emission in a BEC is significant if k_s becomes comparable to the wavevector k_L of the emitted photon since for small momentum transfer $u_{k_L}^2 = k_s^2/k_L^2$.

For comparison, we briefly summarize the suppression of spontaneous emission and light scattering for a fermionic system. A Fermi gas at $T = 0$ with Fermi momentum $\hbar k_F$ is characterized by $N(\mathbf{k}) = \theta(k_F - k)$, i.e., all momentum states with $k < k_F = (6\pi\rho)^{1/3}$ are occupied. If we add an electronically excited atom at rest to the Fermi sea, its spontaneous decay rate is suppressed by a factor

$$F_{\text{Fermi}}^{\text{spont}} = 1 - N(k_L) = \theta(k_L - k_F). \quad (92)$$

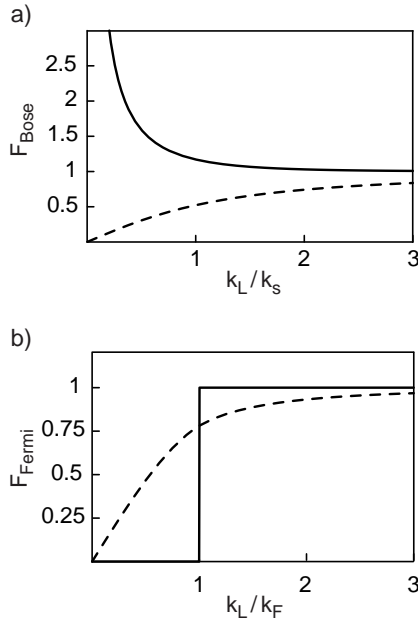


FIG. 25. Modification of spontaneous emission (solid line) and light scattering (dashed line) due to quantum degeneracy. In a) we have plotted the enhancement factor for spontaneous emission and the suppression factor for light scattering for a weakly interacting Bose-Einstein condensate as a function of the light wavevector k_L in units of k_s , the wavevector of an atom moving at the speed of sound. In b) the suppression factors for spontaneous emission and light scattering in a Fermi gas at $T = 0$ are plotted as a function of k_L in units of the Fermi wavevector k_F . Figure is taken from Ref. [16].

When off-resonant light with initial wavevector \mathbf{k}_L is scattered from a filled Fermi sphere into an outgoing wave with final wavevector $\mathbf{k}_L + \mathbf{q}$, the scattering rate is suppressed by [64]

$$\begin{aligned} S_{\text{Fermi}}(\mathbf{q}) &= \int d\mathbf{k} N(\mathbf{k})(1 - N(\mathbf{k} + \mathbf{q})) \\ &= \begin{cases} \frac{3q}{4k_F} - \frac{q^3}{16k_F^3} & \text{if } 0 < q < 2k_F, \\ 1 & \text{if } q > 2k_F. \end{cases} \end{aligned} \quad (93)$$

Eq. 93 is the static structure factor for a Fermi gas at zero temperature. Integrating over all possible scattering angles and accounting for the dipolar emission pattern, we find that the total suppression factor for Rayleigh scattering from a Fermi sea is given by

$$F_{\text{Fermi}}^{\text{scatt}} = \begin{cases} \frac{69}{70} \frac{k_L}{k_F} - \frac{43}{210} \frac{k_L^3}{k_F^3} & \text{if } k_L < k_F \\ 1 - \frac{3}{10} \frac{k_F^2}{k_L^2} + \frac{9}{70} \frac{k_F^4}{k_L^4} - \frac{1}{21} \frac{k_F^6}{k_L^6} & \text{if } k_L > k_F. \end{cases} \quad (94)$$

Fig. 25 shows the influence of quantum degeneracy on the atom-light interaction. Using Eqs. 91, 15, 92, and 94 we have plotted the rates for spontaneous emission (solid lines) and light scattering (dashed lines), normalized by the single-atom rates, for a weakly interacting BEC (Fig. 25a) and a degenerate Fermi gas (Fig. 25b). A significant deviation from the free-particle rate is clearly observable if the photon-momentum is comparable to k_s for bosons and k_F for fermions.

The enhancement of spontaneous emission in a BEC can be intuitively explained as bosonic stimulation by the quantum depletion since the enhancement factor $(1 + N(k_L))$ has the same form as if $N(k_L)$ atoms would occupy the final state. This intuitive argument is correct, but it would incorrectly predict that light *scattering* is also enhanced in contrast to what we have shown in Sect. II. The suppression of light scattering occurs due to the correlation between the admixtures of states with momentum $\hbar\mathbf{k}$ and $-\hbar\mathbf{k}$. This leads to a destructive quantum interference between the two processes $|N, 0, 0\rangle + \hbar\mathbf{q} \rightarrow |N, 1, 0\rangle$ and $|N - 2, 1, 1\rangle + \hbar\mathbf{q} \rightarrow |N, 1, 0\rangle$, in which either an excitation with momentum $\hbar\mathbf{q}$ is created or an excitation with momentum $-\hbar\mathbf{q}$ is annihilated. Both processes transfer momentum $\hbar\mathbf{q}$ to the condensate and are individually enhanced by bosonic stimulation. Therefore, a simple rate equation model would predict enhanced light scattering. However, since the initial states are correlated the two processes leading to the same final state interfere destructively for a BEC with repulsive interactions and light scattering is suppressed.

The static structure factor $S(q)$ of a condensate and the reduced light scattering can be obtained from the Gross-Pitaevskii equation as the response to a periodic perturbation [10]. However, the enhanced spontaneous emission is related to the injection of an additional atom into a condensate and appears to be physics beyond the Gross-Pitaevskii equation.

How strong would the enhancement of spontaneous emission in currently realized Bose-Einstein condensates be? Condensates of ^{23}Na atoms confined in an optical trap have reached a density of $3 \times 10^{15} \text{ cm}^{-3}$ [65]. For this density the speed of sound $\hbar k_s/M = 2.8 \text{ cm/s}$ and the recoil velocity $\hbar k_L/M = 2.9 \text{ cm/s}$ are approximately equal and we find $N(k_L) \approx 0.15$. Thus, the observation of enhanced spontaneous emission in a BEC is within experimental reach. Excited atoms at rest could be produced by injecting ground-state atoms with momentum $\hbar\mathbf{k}_L$ into a condensate and using a counter-propagating laser beam to excite them and bring them to rest. The enhancement of spontaneous emission could then be observed as frequency broadening of the absorption line.

The fact that light scattering is suppressed, but spontaneous emission is enhanced, could be exploited for studies of decoherence in a BEC. When a photon is absorbed by a BEC (the first step of light scattering), it creates a (virtual) excited state that has an external wavefunction which includes pair correlations. Any decoherence of this coherent superposition state, for example by interaction with the thermal cloud, could destroy the interference effect discussed above and turn the suppression of light scattering into an enhancement. Another possibility of creating an excited state atom in a BEC is using Doppler free two-photon excitation, a scheme already used to probe condensates of atomic hydrogen on the $1s \rightarrow 2s$ transition [66]. In this case, enhancement of spontaneous emission could be observed if the excited state lifetime is longer than the coherence time.

X. DOES MATTER WAVE AMPLIFICATION WORK FOR FERMIONS?

Introduction. In the previous sections we have discussed several examples of bosonic stimulation for massive particles, bosonically enhanced elastic collisions, superradiance of atoms [14], and matter wave amplification [17,67]. This and the four wave mixing of atoms [68] were described as processes which are bosonically stimulated, i.e., their rates are proportional to $(N_q + 1)$, where N_q is the number of identical bosons in the final state. These experimental achievements have raised the question whether these processes are inherently connected to bosonic systems.

At the Cargese summer school, we presented the view that all these processes do not depend on Bose-Einstein statistics and would occur for thermal atoms or even for fermions, although with a much shorter coherence time [14]. These suggestions have stirred many controversial discussions at the summer school. This section will reconcile the different physical descriptions. The central result is that the stimulated processes mentioned above do not rely on quantum statistics, but rather on symmetry and coherence. This section is a slightly extended version of a recently submitted paper [69].

We also address a widespread misconception about bosonic stimulation which regards stimulated scattering as being solely due to quantum-statistical enhancement by the final state, i.e., as if the particles in the final state attract other identical particles *without any other physical effect*. We show that the presence of a macroscopically occupied

state increases the density fluctuations of the system, and bosonically enhanced scattering is simply the diffraction of particles from these density fluctuations. First, we establish the equivalence of bosonically enhanced scattering, diffraction and superradiance which will then be applied to fermionic systems.

Scattering theory. Sect. I presented basic aspects of the theory of scattering of light or particles from an arbitrary system. These results simply followed from lowest order perturbation theory (Fermi's Golden Rule). The double differential cross-section for scattering can be decomposed into two factors $\frac{d^2\sigma}{d\Omega d\omega} = \left(\frac{d\sigma}{d\Omega}\right)_{\text{single}} S(q, \omega)$. The first one is the differential cross-section for the scattering by a single particle (e.g. the Rayleigh cross-section for far-off resonant light scattering), the second one is the dynamic structure factor (van Hove or scattering function) $S(q, \omega)$ which is the Fourier transform of the density-density correlation function: $S(q, \omega) = (1/2\pi) \int dt e^{i\omega t} \langle \hat{\rho}(q, t) \hat{\rho}^\dagger(q, 0) \rangle$ where $\hat{\rho}(q)$ is the Fourier transform of the particle density operator introduced in Sect. I.

For a non-interacting system of bosons, $S(q, \omega)$ can be expressed using the single-particle states $|i\rangle$ with energy E_i and occupation numbers N_i as

$$S(q, \omega) = S_0(q) \delta(\omega) + \sum_{i \neq j} |\langle j | e^{iqr} | i \rangle|^2 N_i (N_j + 1) \delta[\omega - (E_j - E_i)/\hbar]. \quad (95)$$

The factor $(N_j + 1)$ reflects bosonic stimulation by the occupation of the final state. We have split off the elastic term $S_0(q)$ which describes coherent elastic scattering or diffraction and is simply the square of the Fourier transform of the density $S_0(q) = |\langle \rho^\dagger(q) \rangle|^2 = |\sum N_i \langle i | e^{iqr} | i \rangle|^2$.

A simple example. It is instructive to apply this formalism to a system of non-interacting bosons which has macroscopic occupation in two momentum states with momentum $\pm \hbar \mathbf{k}$. If the initial state is a Fock state $|+k\rangle^{N_+} |-k\rangle^{N_-}$, we find that, apart from forward scattering, the dominant term in $S(q, \omega)$ is the bosonically enhanced scattering between those two (degenerate) states, $S(q, \omega) = [N^2 \delta_{q,0} + N_+(N_- + 1) \delta_{q,-2k} + N_-(N_+ + 1) \delta_{q,2k}] \delta(\omega)$ where the Kronecker symbol $\delta_{q,p}$ implies $\mathbf{q} = \mathbf{p}$ within the wavevector resolution $\approx 1/l$ of a finite volume with length l . Alternatively, we can assume the initial state to be a coherent superposition state $|i\rangle^N$ with the eigenstate $|i\rangle = c_+ | +k \rangle + c_- | -k \rangle$ and $|c_\pm|^2 = N_\pm/N$ and $N = N_+ + N_-$. Now, the dominant contribution to $S(q, \omega)$ comes from $S_0(q) = N^2 \delta_{q,0} + N^2 |c_+|^2 |c_-|^2 [\delta_{q,2k} + \delta_{q,-2k}]$ which is equivalent to the Fock state case when the difference between N_\pm and $N_\pm + 1$ can be neglected in the limit of large occupation numbers.

This equivalence between Fock states and coherent superposition states has been extensively discussed in the context of two interfering Bose-Einstein condensates [70–72] and also with regard to optical coherences [73]. Those papers show that, in many situations, a Fock state is equivalent to an ensemble of coherent states with arbitrary phase. Experimental interrogation determines the phase and reduces the ensemble to a single coherent state with a phase which will vary from experiment to experiment. For large occupation numbers, one can therefore regard the Fock state as an initial state which has not yet “declared its phase”, and, in many cases, for the convenience of calculations, replace the Fock state by a coherent superposition state with an arbitrarily chosen phase.

However, on first sight, the physical interpretation is different. In the Fock state formulation, the enhanced scattering results from a macroscopic occupation number in a single quantum state, whereas for the coherent superposition state, the scattering is simple diffraction by a sinusoidally modulated density distribution with an amplitude proportional to $N|c_+c_-|$. This density modulation acts as a diffraction grating for incident light or particles and has a diffraction efficiency proportional to the square of the amplitude. Such a density modulation does not require bosonic atoms. It can, for example, be imprinted into thermal or fermionic clouds by subjecting them to a suitable optical standing wave. The equivalence of these two descriptions points towards one of the major conclusions of this section, namely that macroscopic population of bosonic states is not necessary for enhanced scattering.

The previous discussion assumed scattering between two degenerate momentum states $|\pm k\rangle$. A simple Galilean transformation generalizes this to two arbitrary momentum states $|k_\pm\rangle$ with energies E_\pm . Now the standing wave moves with a velocity $\hbar(k_+ + k_-)/2M$ where M is the mass of the atoms, and the enhanced scattering appears at $\hbar\omega = \pm(E_+ - E_-)$ instead of at $\omega = 0$.

Enhancement of fluctuations. The general results of statistical physics presented above emphasize that enhanced scattering *must* be related to enhanced density fluctuations. Therefore, bosonic enhancement of a scattering rate is either due to a density modulation $\langle \rho(q) \rangle$ (in the coherent superposition description) or due to density fluctuations (in the Fock state description)—the latter can be regarded as a density modulation with an unknown phase. This relation allows a more intuitive answer to the question why is there bosonic enhancement when two atoms 1 and 2 collide in the presence of a condensate with N_0 atoms. The standard answer would be that the symmetry of the wavefunction enhances the scattering rate into the condensate and into some other state 3 by a factor of $(N_0 + 1)$. An

equivalent answer is that the condensate interferes with atom 2 (or 1) and creates a density grating with an amplitude proportional to $N_0^{1/2}$ which diffracts atom 1 (or 2) into state 3. The grating absorbs this momentum transfer by transferring the atom in state 2 (or 1) into the condensate. Therefore, bosonic stimulation can be regarded as heterodyne amplification of density fluctuations where the condensate acts as the local oscillator. This alternative physical picture emphasizes the role of interference in bosonic stimulation.

Dicke superradiance. We now want to establish the connection between bosonic enhancement and Dicke superradiance. This will formally introduce the enhancement factor $(N + 1)$ for non-bosonic systems. A system with N atoms in two states $|\pm\rangle$ is conveniently described with the formalism introduced by Dicke to discuss superradiance in two-level atoms [74]. It should be emphasized that the only assumption in this treatment is that the N atoms couple identically to the probe field (the electromagnetic field or some incident particle beam), i.e., that they have the same transition frequency and matrix element without any assumption of quantum statistics. For example, in magnetic resonance experiments, the Dicke treatment would apply to different atomic species with the same value of the magnetic moment.

It should be emphasized that Dicke superradiance depends only on the symmetry of the emitting system and does not depend on the nature of the emitted particle, whether they are bosons or fermions. For example, the Dicke treatment would apply to an ensemble of atoms in an autoionizing state which emit electrons. If the ensemble is localized within a de Broglie wavelength of the electron, enhanced superradiant emission would occur. The fermionic nature of the emitted particles is irrelevant in the so-called microscopic regime [52] where less than one emitted particle is in the volume of the sample. This is the situation originally discussed by Dicke. Many experiments on superradiant emission of light have been done in regimes with many photons per mode which of course would not be possible with fermions.

Dicke treated the two-level atom as a spin $1/2$ system and introduced angular momentum quantum numbers. In this subspace, a fully symmetric state of N atoms has spin $s = N/2$ and magnetic quantum number $m = (N_+ - N_-)/2$. The squared matrix element for the transition $|s, m \pm 1\rangle \rightarrow |s, m\rangle$ induced by the ladder operator S_{\mp} is $(s \pm m + 1)(s \mp m)$. Expressing this by initial occupation numbers N_{\pm} , one obtains $N_{\pm}(N_{\mp} + 1)$ [75–77] retrieving the formula of bosonic enhancement. The transition rates are largest for the N particle state with $s = N/2$ which is therefore called the state of maximum cooperativity.

Such a system will couple to the probe field in a superradiant way (i.e. with an up to N times enhanced transition rate). In the Bloch vector picture, its dynamics is described as the precession of a macroscopic spin vector with length $s = N/2$. This spin vector decays in a time $1/\Gamma$ where Γ is the total (homogeneous and inhomogeneous) linewidth of the transition $|+\rangle \rightarrow |-\rangle$. Collective superradiant behaviour can only be observed at times shorter than $1/\Gamma$.

Matter wave gratings and fermions. Dicke's formalism is usually applied to one-photon transitions between internal states, but here we use it to discuss scattering, i.e., a two-photon transition between two momentum states $|k_{\pm}\rangle$. Let's first assume that we have an ideal Bose-Einstein condensate in the $\mathbf{k} = 0$ momentum state. Light scattering between momentum states $\mathbf{k} = 0$ and $\mathbf{k} = \mathbf{q}$ has an infinite coherence time for a non-interacting condensate of infinite size (Fig. 26a). For a thermal (non-degenerate) cloud of atoms with thermal momentum spread $\hbar k_{\text{th}} \ll \hbar q$ the transition for the transfer of momentum $\hbar q$ is Doppler broadened by $\Gamma = \hbar k_{\text{th}} q / m$. For times shorter than $1/\Gamma$ the system will behave collectively like the Bose condensed system, i.e., a probe beam would induce transitions between the $\mathbf{k} = 0$ and $\mathbf{k} = \mathbf{q}$ momentum states at a rate proportional to $N_{k=0}(N_{k=q} + 1)$ where $N_{k=0,q}$ refers to the total number of atoms in states with momentum around $\mathbf{k} = 0, \mathbf{q}$.

Once we have distributed the particles over many initial states, indistinguishability and quantum statistics don't play any role. Therefore, the only modification for a Fermi degenerate cloud is to replace k_{th} with the Fermi wavevector k_F in the expression for the inhomogeneous broadening (Fig. 26b). Due to the assumption $\hbar k_F \ll \hbar q$, Pauli blocking due to scattering into already occupied states is absent. If this assumption is not made, a part of the cloud becomes inactive, and our discussion would apply only to the atoms near the Fermi surface.

The previous paragraph generalized the bosonic *Fock state* ensemble to non-degenerate and fermionic clouds. We now come back to the *coherent superposition* state. For bosons, it can be produced from a Bose-Einstein condensate in the $\mathbf{k} = 0$ state by applying a (so-called Bragg) pulse of two laser beams which differ in wavevector by \mathbf{q} and in frequency by the recoil frequency $\hbar q^2 / 2m$. Those beams resonantly drive the transition between momentum states $\mathbf{k} = 0$ and $\mathbf{k} = \mathbf{q}$ [78,20] and prepare the superposition state discussed above. Similarly, in a thermal (or fermionic) cloud, the Bragg pulse creates a modulated density distribution with wavelength $2\pi/q$ which has the same contrast as in the bosonic case and will diffract light or atoms at the same rate. However, due to the thermal motion with velocity $\hbar k_{\text{th}} / M$, this grating decays during a time $M / \hbar k_{\text{th}} q = 1/\Gamma$ (for the fermionic case, k_F has to be substituted for k_{th}). Thus the Dicke picture and the diffraction picture agree.

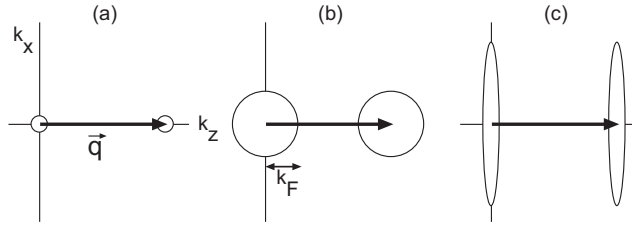


FIG. 26. Momentum transfer \mathbf{q} (a) to a Bose-Einstein condensate, (b) to a Fermi sea, and (c) to a momentum squeezed degenerate Fermi cloud. Shown are the populated states vs. the k -vector. The momentum spread k_F of the Fermi sea introduces Doppler broadening of the transition and a finite coherence time, whereas the coherence time in (a) and (c) is infinite. Figure is taken from Ref. [69].

Coherence time. The Doppler broadening discussed above seems to imply a fundamental limit to the coherence time of a Fermi system. However, at least in principle, one can prepare a Fermi system with infinite coherence time by starting out with a cloud which is in a single momentum state along the \hat{z} axis, but occupies many momentum states along \hat{x} and \hat{y} . With a Bragg pulse transferring momentum $\hbar q \hat{z}$, one can prepare a system which shows collective behavior for scattering particles or light with momentum transfer $\hbar q \hat{z}$ with an infinite coherence time (Fig. 26c). Therefore, there is no direct connection between a long coherence time and a high phase-space density. In this ensemble, the scattering is between the states $|k_z = 0\rangle \otimes |k_x, k_y\rangle$ and $|k_z = q\rangle \otimes |k_x, k_y\rangle$. Therefore, we have enhanced scattering into the $|k_z = q\rangle$ quantum state, but the atoms may differ in other quantum numbers. What matters is only the symmetrization of the many-body wavefunction along \hat{z} . The other quantum numbers ensure that there is no conflict with the Pauli blocking for fermionic systems. This is analogous to the separation of electronic wavefunctions into a symmetric part (e.g. the spin part) and an antisymmetric part (e.g. the spatial part) where the coupling to an external field (e.g. electron spin resonance experiment) only depends on the symmetric part.

Experiments. The experiments both on superradiance (Sect. VII and [14]) and four-wave mixing [68] in Bose-Einstein condensates have in common that a matter wave grating formed by two macroscopically occupied momentum states is probed, either by light or by atoms. Both experiments create the coherent superposition state discussed above using a Bragg pulse. In the limit of low intensity of the probe beam, the scattering is independent of the nature of the probe particles—one could have used any kind of radiation, bosons or fermions [79]. The bosonic stimulation observed in both experiments demonstrates the dynamic nature of the matter wave grating. Each time, a particle or photon is diffracted, the amplitude of the grating grows.

In practice, it is difficult or impossible to carry out these experiments with fermions or thermal atoms. When we observed superradiance of a condensate, we couldn't observe similar behaviour above the BEC transition temperature since the threshold laser intensity for superradiant gain is several orders of magnitude higher (see Ref. [14] for details). Furthermore, the superradiance may be suppressed by heating or other decoherence processes. The shorter coherence time for non-BEC samples should be even more crucial for the four-wave mixing experiment where the matter wave grating is probed by very slow atoms which have a long transit time of about 1 ms through the sample. Another concern are incoherent processes which accompany the stimulated processes discussed so far. Since the incoherent processes scale linearly with the number of atoms, whereas the stimulated process is proportional to N^2 , there is in principle always a regime where the stimulated process dominates³.

Discussion. Coming back to the initial question: Is matter wave amplification possible for fermions? The answer is yes, if the system is prepared in a cooperative state and the amplification is faster than the coherence time. However, this amplification does not pile up atoms in a single quantum state, but rather in states which are in the same (or approximately the same) momentum state along \hat{z} , but differ in other quantum numbers. Therefore, this amplification can be regarded as amplification of a density modulation or as amplification of spatial bunching of atoms. Alternatively, one can regard the density modulation as a collective excitation of the system which involves bosonic quasi-particles (e.g. phonons). Superradiance and four-wave mixing (both with bosons and fermions) can then be ascribed to bosonic stimulation by those quasi-particles.

³In the case of a fermionic sample, the density of particles can only be increased by increasing the momentum spread of the sample. This can increase the incoherent “background” for four-wave mixing. For the ensemble in Fig. 26c an increase in N at constant volume requires the transverse velocity spread to increase as $N^{1/2}$. Therefore, for large N , the incoherent elastic scattering rate increases as $N^{3/2}$, still more slowly than the stimulated scattering.

The phase-coherent matter wave amplification for fermions would start with a short Bragg pulse which puts some of the atoms into a recoil state which is then amplified. This superposition of two momentum states creates a matter wave grating. This can be regarded as the interference pattern of each atom with itself with all the individual interference patterns being exactly in phase. Matter wave amplification occurs when a single laser beam is diffracted off this grating increasing the amplitude of each atom to be in the recoiling state. Therefore, the matter wave amplification scheme of Refs. [17,67] would work for fermions, provided the whole process can be done in the short coherence time of the fermionic matter wave grating.

Of course, there is a fundamental difference between bosons and fermions which is reflected in the symmetry of the total wavefunction. A bosonic system with two macroscopically occupied quantum states is *always* in a fully symmetric and maximally cooperative state. In other words, if two independent Bose condensates cross each other, there is always a macroscopic interference pattern (as observed experimentally [24]), which is reflected in $S(q, \omega)$ being proportional to N^2 (or to N_+N_- , to be more precise). It is this density modulation which can be amplified by the dynamic diffraction discussed in this paper. If two beams of fermions overlap, there is no macroscopic interference, unless the two beams were prepared in a symmetric way, e.g. by generating one of the beams by a Bragg pulse from the other one.

Our discussion of scattering without change of the internal state can be generalized. For example, if atoms scatter into the condensate through a spinflip process, the density grating has to be replaced by a polarization or coherence grating. Such gratings were experimentally studied for laser-cooled atoms [80].

This discussion has focused on bosonically enhanced *scattering*. Similarly, bosonic enhancement of spontaneous emission depends only on a cooperative initial state and not directly on quantum statistics. For scattering, the relevant coupling strength are the density fluctuations. For spontaneous emission, it is the electric dipole moment. Both are enhanced by the presence of a Bose condensate, in the latter case because the excited atom corresponds to a Dicke vector of spin $s = N/2, m = -(N/2) + (1/2)$ which couples more strongly to the vacuum fluctuations of the electromagnetic field than an individual atom. Alternatively, the enhanced spontaneous emission can be regarded as the constructive interference of an “emitted” ground state atom with the macroscopic ground state matter wave. This picture is analogous to the semi-classical interpretation of stimulated emission of light. Ref. [75] shows that bosonic stimulation of photons is due to the constructive interference of the emission of a classical oscillating dipole with the incident field in the forward direction.

XI. DISCUSSION

This paper has summarized our recent experiments on Bose-Einstein condensation with the unifying theme of enhancement and suppression. Suppression of scattering or dissipation can arise for two different reasons. The phonon and vortex nature of the collective excitations together with energy and momentum conservation allow dissipation only above a critical velocity. In addition, one has to consider the dynamics of the excitation process. For microscopic particles, this is reflected in the matrix element $S(q)$ which characterizes how easily can the condensate absorb momentum in a scattering process. For macroscopic motion, it is reflected in a critical velocity for vortex nucleation. Scattering processes are also enhanced by the population of the final states (bosonic stimulation). Optical stimulation by a laser beam was used in Bragg scattering, and matter wave stimulation led to superradiance and matter wave amplification.

We have also discussed some subtleties which go beyond the simple picture using rate equations and occupation numbers. A condensate in its ground state is in a coherent superposition state of the zero-momentum state with correlated pairs with momenta $\pm \mathbf{q}$ (the quantum depletion). We have shown that the population in the quantum depletion can cause bosonic stimulation of spontaneous emission. However, for a scattering situation, there are two bosonically enhanced pathways which destructively interfere (causing $S(q) < 1$). Therefore, the concept of bosonic stimulation can be applied to the many-body state of a condensate, but with caution. Finally, we have shown that some form of matter wave amplification is possible in fermionic samples. This required a careful discussion of bosonic stimulation by particles vs. quasi-particles and the role of symmetry vs. quantum degeneracy.

In closing we want to point out that the rich and complex physics displayed here is based essentially on two four-wave mixing Hamiltonians. One describes s -wave interaction of the condensate which is responsible for all the many-body effects discussed here including superfluidity. The other one couples the atoms to the light (or impurity atoms) and led to superradiance and amplification of light and atoms.

We are grateful to Alain Aspect, Jean Dalibard, William D. Phillips, Gora Shlyapnikov, and Philippe Bouyer for organizing a stimulating summer school, to Ananth Chikkatur for contributions to the sections on collisions, and to

Axel Görlitz and Aaron Leanhardt for valuable comments on the manuscript. This work was supported by NSF, ONR, ARO, NASA, and the David and Lucile Packard Foundation.

- [1] F. London, *Superfluids, Vol. II* (Dover, New York, 1964).
- [2] K. Huang, *Statistical Mechanics* (Wiley, New York, 1987).
- [3] N. N. Bogoliubov, J. Phys. (USSR) **11**, 23 (1947).
- [4] M. H. Anderson, J. R. Ensher, M. R. Matthews, C. E. Wieman, and E. A. Cornell, Science **269**, 198 (1995).
- [5] K. B. Davis, M.-O. Mewes, M. A. Joffe, M. R. Andrews, and W. Ketterle, Phys. Rev. Lett. **74**, 5202 (1995).
- [6] C. C. Bradley, C. A. Sackett, J. J. Tollet, and R. G. Hulet, Phys. Rev. Lett. **75**, 1687 (1995).
- [7] F. Dalfovo, S. Giorgini, L. P. Pitaevskii, and S. Stringari, Rev. Mod. Phys. **71**, 463 (1999).
- [8] W. Ketterle and N. J. van Druten, in *Advances in Atomic, Molecular, and Optical Physics*, edited by B. Bederson and H. Walther (Academic Press, San Diego, 1996), Vol. 37, pp. 181–236.
- [9] W. Ketterle, D. S. Durfee, and D. M. Stamper-Kurn, in *Bose-Einstein condensation in atomic gases, Proceedings of the International School of Physics Enrico Fermi, Course CXL*, edited by M. Inguscio, S. Stringari, and C. Wieman (IOS Press, Amsterdam, 1999), pp. 67–176. e-print arXiv:cond-mat/9904034 .
- [10] D. Stamper-Kurn and W. Ketterle, in *Coherent Atomic Matter Waves*, Proceedings of the Les Houches Summer School, Course LXXII in 1999, edited by R. Kaiser, C. Westbrook, and F. David (Springer, New York, 2001), e-print arXiv:cond-mat/0005001 .
- [11] A. P. Chikkatur, A. Görlitz, D. M. Stamper-Kurn, S. Inouye, S. Gupta, and W. Ketterle, Phys. Rev. Lett. **85**, 483 (2000).
- [12] C. Raman, M. Köhl, R. Onofrio, D. S. Durfee, C. E. Kuklewicz, Z. Hadzibabic, and W. Ketterle, Phys. Rev. Lett. **83**, 2502 (1999).
- [13] R. Onofrio, C. Raman, J. M. Vogels, J. Abo-Shaeer, A. P. Chikkatur, and W. Ketterle, Phys. Rev. Lett. **85**, 2228 (2000).
- [14] S. Inouye, A. P. Chikkatur, D. M. Stamper-Kurn, J. Stenger, D. E. Pritchard, and W. Ketterle, Science **285**, 571 (1999).
- [15] D. M. Stamper-Kurn, A. P. Chikkatur, A. Görlitz, S. Inouye, S. Gupta, D. E. Pritchard, and W. Ketterle, Phys. Rev. Lett. **83**, 2876 (1999).
- [16] A. Görlitz, A. P. Chikkatur, and W. Ketterle, Phys. Rev. A, in print; cond-mat/ 0008067.
- [17] S. Inouye, T. Pfau, S. Gupta, A. P. Chikkatur, A. Görlitz, D. E. Pritchard, and W. Ketterle, Nature **402**, 641 (1999).
- [18] S. Inouye, R.F.Löw, S. Gupta, T. Pfau, A. Görlitz, T. L. Gustavson, D. E. Pritchard, and W. Ketterle, Phys. Rev. Lett. **85**, 4225 (2000).
- [19] M. O. Mewes, M. R. Andrews, N. J. van Druten, D. M. Kurn, D. S. Durfee, and W. Ketterle, Phys. Rev. Lett. **77**, 416 (1996).
- [20] J. Stenger, S. Inouye, A. P. Chikkatur, D. M. Stamper-Kurn, D. E. Pritchard, and W. Ketterle, Phys. Rev. Lett. **82**, 4569 (1999).
- [21] F. Zambelli, L. Pitaevskii, D. M. Stamper-Kurn, and S. Stringari, Phys. Rev. A **61**, 063608 (2000).
- [22] P. J. Price, Phys. Rev. **94**, 257 (1954).
- [23] A. Griffin, *Excitations in a Bose-condensed liquid* (Cambridge University Press, Cambridge, 1993).
- [24] M. R. Andrews, C. G. Townsend, H.-J. Miesner, D. S. Durfee, D. M. Kurn, and W. Ketterle, Science **275**, 637 (1997).
- [25] R. J. Ballagh, K. Burnett, and T. F. Scott, Phys. Rev. Lett. **78**, 1607 (1997).
- [26] Y. B. Band, P. S. Julienne, and M. Trippenbach, Phys. Rev. A **59**, 3823 (1999).
- [27] Y. B. Band, M. Trippenbach, J. P. Burke Jr., and P. S. Julienne, Phys. Rev. Lett. **84**, 5462 (2000).
- [28] L. D. Landau, J. Phys. (USSR) **5**, 71 (1941).
- [29] L. Meyer and F. Reif, Phys. Rev. **123**, 727 (1961).
- [30] D. R. Allum, P. V. E. McClintock, A. Phillips, and R. M. Bowley, Phil. Trans. R. Soc. A **284**, 179 (1977).
- [31] J. Harms and J. P. Toennies, Phys. Rev. Lett. **83**, 344 (1999).
- [32] E. W. Hagley, L. Deng, M. Kozuma, J. Wen, K. Helmerson, S. L. Rolston, and W. D. Phillips, Science **283**, 1706 (1999).
- [33] A. I. Lvovsky and S. R. Hartmann, Phys. Rev. Lett. **82**, 4420 (1999).
- [34] P. Nozières and D. Pines, *The Theory of Quantum Liquids* (Addison-Wesley, Redwood City, CA, 1990).
- [35] M. Crescimanno, C. G. Koay, R. Peterson, and R. Walsworth, Phys. Rev. A **62**, 063612 (2000).
- [36] R. P. Feynman, in *Progress in Low Temperature Physics*, edited by C. Gorter (North-Holland, Amsterdam, 1955), Vol. 1, p. 17.
- [37] E. Lundh, C. J. Pethick, and H. Smith, Phys. Rev. A **55**, 2126 (1997).
- [38] K. W. Madison, F. Chevy, W. Wohlleben, and J. Dalibard, Phys. Rev. Lett. **84**, 806 (2000).
- [39] D. L. Feder, C. W. Clark, and B. I. Schneider, Phys. Rev. A **61**, 011601(R) (1999).
- [40] T. Isoshima and K. Machida, Phys. Rev. A **60**, 3313 (1999).
- [41] B. Jackson, J. F. McCann, and C. S. Adams, Phys. Rev. A **61**, 051603(R) (2000).

- [42] T. Frisch, Y. Pomeau, and S. Rica, *Phys. Rev. Lett.* **69**, 1644 (1992).
- [43] B. Jackson, J. F. McCann, and C. S. Adams, *Phys. Rev. Lett.* **80**, 3903 (1998).
- [44] T. Winiecki, J. F. McCann, and C. S. Adams, *Phys. Rev. Lett.* **82**, 5186 (1999).
- [45] C. Raman, R. Onofrio, J. M. Vogels, J. R. Abo-Shaeer, and W. Ketterle, preprint cond-mat/0008423.
- [46] N. E. Rehler and J. H. Eberly, *Phys. Rev. A* **3**, 1735 (1971).
- [47] R. H. Dicke, in *Quantum Electronics, Proceedings of the third international congress*, edited by P. Grivet and N. Bloembergen (Columbia University Press, New York, 1964), p. 35.
- [48] L. Casperson and A. Yariv, *Phys. Rev. Lett.* **26**, 293 (1971).
- [49] S. Chu and S. Wong, *Phys. Rev. Lett.* **48**, 738 (1982).
- [50] L. V. Hau, S. E. Harris, Z. Dutton, and C. H. Behroozi, *Nature* **397**, 594 (1999).
- [51] C. Cohen-Tannoudji, J. Dupont-Roc, and G. Grynberg, *Atom-Photon Interactions* (Wiley, New York, 1992).
- [52] M. Gross and S. Haroche, *Phys. Rep.* **93**, 301 (1982).
- [53] M. P. van Exter, S. J. M. Kuppens, and J. P. Woedman, *Phys. Rev. A* **51**, 809 (1995).
- [54] M. G. Moore and P. Meystre, *Phys. Rev. Lett.* **83**, 5202 (1999).
- [55] J.-Y. Courtois, G. Grynberg, B. Lounis, and P. Verkerk, *Phys. Rev. Lett.* **72**, 3017 (1994).
- [56] R. Bonifacio and L. D. Salvo, *Nuclear Instruments and Methods in Physics Research A* **341**, 360 (1994).
- [57] G. L. Lippi, G. P. Barozzi, S. Barbay, and J. R. Tredicce, *Phys. Rev. Lett.* **76**, 2452 (1996).
- [58] P. R. Hemmer, N. P. Bigelow, D. P. Katz, M. S. Shahriar, L. DeSalvo, and R. Bonifacio, *Phys. Rev. Lett.* **77**, 1468 (1996).
- [59] W. J. Brown, J. R. Gardner, D. J. Gauthier, and R. Vilaseca, *Phys. Rev. A* **55**, R1601 (1997).
- [60] M. G. Moore and P. Meystre, *Phys. Rev. A* **59**, 1754 (1999).
- [61] P. R. Berman, *Phys. Rev. A* **59**, 585 (1999).
- [62] H. A. Haus, *Waves and Fields in Optoelectronics* (Prentice-Hall, Englewood Cliffs, NJ, 1984).
- [63] S. E. Harris and L. V. Hau, *Phys. Rev. Lett.* **82**, 4611 (1999).
- [64] D. Pines and P. Nozières, *The Theory of Quantum Liquids, Vol. 1* (Addison-Wesley, Reading, MA, 1988).
- [65] D. M. Stamper-Kurn, M. R. Andrews, A. P. Chikkatur, S. Inouye, H.-J. Miesner, J. Stenger, and W. Ketterle, *Phys. Rev. Lett.* **80**, 2027 (1998).
- [66] D. G. Fried, T. C. Killian, L. Willmann, D. Landhuis, S. C. Moss, D. Kleppner, and T. J. Greytak, *Phys. Rev. Lett.* **81**, 3811 (1998).
- [67] M. Kozuma, Y. Suzuki, Y. Torii, T. Sugiura, T. Kuga, E. W. Hagley, and L. Deng, *Science* **286**, 2309 (1999).
- [68] L. Deng, E. W. Hagley, J. Wen, M. Trippenbach, Y. Band, P. S. Julienne, J. E. Simsarian, K. Helmerson, S. L. Rolston, and W. D. Phillips, *Nature* **398**, 218 (1999).
- [69] W. Ketterle and S. Inouye, preprint, cond-mat/0008232.
- [70] J. Javanainen and S. M. Yoo, *Phys. Rev. Lett.* **76**, 161 (1996).
- [71] M. Naraschewski, H. Wallis, A. Schenzle, J. I. Cirac, and P. Zoller, *Phys. Rev. A* **54**, 2185 (1996).
- [72] Y. Castin and J. Dalibard, *Phys. Rev. A* **55**, 4330 (1997).
- [73] K. Mølmer, *Phys. Rev. A* **55**, 3195 (1997).
- [74] R. H. Dicke, *Phys. Rev.* **93**, 99 (1954).
- [75] M. Sargent III, M. O. Scully, and J. W. E. Lamb, *Laser Physics* (Addison Wesley, Reading, Massachusetts, 1974).
- [76] J. J. Sakurai, *Modern Quantum Mechanics* (Addison-Wesley, Reading, Massachusetts, 1994).
- [77] H. Wallis, *Appl. Phys. B* **65**, 707 (1997).
- [78] M. Kozuma, L. Deng, E. W. Hagley, J. Wen, R. Lutwak, K. Helmerson, S. L. Rolston, and W. D. Phillips, *Phys. Rev. Lett.* **82**, 871 (1999).
- [79] P. Villain, P. Öhberg, L. Santos, A. Sanpera, and M. Lewenstein, preprint cond-mat/0005417.
- [80] A. Kumarkrishnan, S. B. Cahn, U. Shim, and T. Sleator, *Phys. Rev. A* **58**, R3387 (1998).